

**A STUDY OF CIRCUMFERENTIAL  
WRINKLES IN ROLLS OF WEB**

By

JOHN MICHAEL HIX

Bachelor of Science

Oklahoma State University

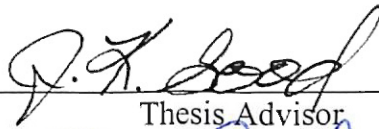
Stillwater, Oklahoma

2002

Submitted to the Faculty of the Graduate College of  
Oklahoma State University in partial fulfillment  
of the requirements for the Degree of  
MASTER OF SCIENCE  
May, 2004

A STUDY OF CIRCUMFERENTIAL  
WRINKLES IN ROLLS OF WEB


Thesis Approved:

  
\_\_\_\_\_

Thesis Advisor

  
\_\_\_\_\_

  
\_\_\_\_\_

  
\_\_\_\_\_

Dean of the Graduate College

## **ACKNOWLEDGMENTS**

First, I would first like to thank my wife, Tara, for her devoted love and support. Thank you for being my best friend for the last nine years of my life. Second, I would like to thank Dr. Good for giving me the opportunity to work for him. It is with your constant help and advice that made it possible for me to finish graduate school in such a timely manner. Next, I would like to thank my coworkers. When I came to a slow point in my project or when I was just having a bad day, it really helped to have great people to talk with. I also owe a big thanks to my parents. You bought me my first set of building blocks, and when you saw that I had a great interest in design, you encouraged me throughout my life to seek my dream of becoming an engineer. Finally, I would like to thank all of my other friends and family. Thank you for being understanding when I was too busy to accept your invitations, and thank you for your love and encouragement.

## TABLE OF CONTENTS

<b>CHAPTER 1</b> .....	<b>1</b>
<b>INTRODUCTION</b> .....	<b>1</b>
Background .....	1
Sources of CMD Stress .....	1
Purpose of Project .....	2
<b>CHAPTER 2</b> .....	<b>3</b>
<b>LITERATURE SURVERY</b> .....	<b>3</b>
<b>CHAPTER 3</b> .....	<b>10</b>
<b>THEORETICAL DEVELOPMENT</b> .....	<b>10</b>
Introduction to Models.....	10
Axially Compressed Cylindrical Shell Models.....	10
Shell on Elastic Foundation Model.....	11
Shell on Rigid Core with External Pressure Model .....	14
Axial Compression with Apparatus Effects Model .....	15
<b>CHAPTER 4</b> .....	<b>19</b>
<b>EXPERIMENTAL SETUP AND PROCEDURE</b> .....	<b>19</b>
Machine Setup .....	19
Core Design .....	20
Experimental Procedure.....	24
Preliminary Tests .....	26
Primary Tests .....	29
<b>CHAPTER 5</b> .....	<b>31</b>
<b>RESULTS AND DISCUSSION</b> .....	<b>31</b>
Flat Core Analysis and Discussion .....	32
Toothed Core Analysis and Discussion .....	37
<b>CHAPTER 6</b> .....	<b>50</b>
<b>CONCLUSIONS AND FUTURE WORK</b> .....	<b>50</b>
Conclusions.....	50
Future Work.....	51
<b>REFERENCES</b> .....	<b>52</b>

## LIST OF TABLES

Table 4-1: Dimensions of Cores .....	24
Table 4-2: Results from Preliminary Tests .....	26
Table 4-3: Radial Elastic Modulus and Pressures Found Using Winder .....	29
Table 4-4: List of Primary Tests Performed .....	29
Table 4-5: List of Material Properties .....	30
Table 5-1: Descriptions of Theoretical Models .....	31
Table 5-2: Critical Forces Found for Tests Conducted on the Flat Core .....	34
Table 5-3: Critical Forces Found for Tests Conducted on Toothed Core #2 .....	44

## LIST OF FIGURES

Figure 3-1: Diagram of Cylindrical Shell on an Elastic Foundation Model.....	11
Figure 3-2: Model of Cylinder on Rigid Core with Pressure.....	15
Figure 3-3: Toothed Core with Dimensions of Contact Area of Teeth Labeled .....	17
Figure 4-1: Labeled Setup of Winding Machine .....	20
Figure 4-2: 3-D Model of Flat Core.....	21
Figure 4-3: Photograph of Flat Core and Spacers.....	22
Figure 4-4: 3-D Model of Toothed Core.....	23
Figure 4-5: Photograph of Toothed Core and Spacers.....	23
Figure 4-6: Setup of Web Path.....	25
Figure 4-7: Plot of Stretch Test Performed on 142 Gauge Polyester Film.....	27
Figure 4-8: Plot of Pfeiffer's Equation and Results of Stack Test.....	28
Figure 5-1: Buckling Shape Resulting from Flat Core Tests.....	32
Figure 5-2: Example Buckling Curve for Flat Core .....	33
Figure 5-3: Comparison of Experimental Flat Core Data to Model #1 .....	35
Figure 5-4: Comparison of Experimental Flat Core Data to Model 2 .....	36
Figure 5-5: Imperfections Seen in Rolls After Winding.....	37
Figure 5-6: Pre-buckling that Occurs in the Gaps of Toothed Core #1 .....	38
Figure 5-7: Main Buckling Shape Seen with Toothed Core #1 .....	39
Figure 5-8: Example Buckling Curves for Toothed Core #1 .....	40

Figure 5-9: Comparison of Toothed Core #1 data to Model #2 .....	41
Figure 5-10: Example Buckling Curve for Toothed Core #2 .....	42
Figure 5-11: Buckle Shape Seen for Test Conducted on Toothed Core #2 .....	42
Figure 5-12: Toothed Core #2 Initial Tests Compared to Toothed Core #1 .....	43
Figure 5-13: Averaged Results of Toothed Core #2 Tests .....	44
Figure 5-14: Comparison of Toothed Core #2 Data to Model #3.....	46
Figure 5-15: Frictional Force between the Teeth Compared to Web Tension .....	47
Figure 5-16: Comparison of Toothed Core #2 Data to Model #5.....	48

## NOMENCLATURE

CMD	Cross Machine Direction
MD	Machine Direction
E	Elastic Modulus
$E_r$	Radial Elastic Modulus
$\nu$	Poisson's Ratio
D	Flexural Rigidity
m	Longitudinal Half Wave Number
n	Circumferential Half Wave Number
l	Length of Cylinder
h	Thickness of Shell
r	Radius
d	Diameter
$r_o$	Web Roll Outer Radius
$r_i$	Web Roll Inner Radius
t	Foundation Thickness
$P_x$	Force
$P_{cr}$	Critical Force
$N_x$	Force per Length
$N_{cr}$	Critical Force per Length



$\sigma_x$	Stress
$\sigma_{cr}$	Critical Stress
$\sigma_t$	Hoop Stress
k	Foundational Stiffness
A	Area
p	Pressure
I	Moment of Inertia
$\Delta$	Deformation of Elastic Foundation
C	Constant
$A_c$	Area of Contact between Sides of Teeth
$F_{fric}$	Frictional Force between Sides of Teeth
$\mu$	Friction Coefficient
$\pi$	Pi (3.1416)
w	Direction Perpendicular to Axis
x	Direction on Shell Surface, Parallel to Axis
lb/lbs	Pounds
in	Inches
psi	Pounds per Inches Squared
FEM	Finite Element Method
WHRC	Web-Handling Research Center

# CHAPTER 1

## INTRODUCTION

### Background

Axisymmetric buckles that form on wound rolls are a common problem that occur in the web-handling industry. These wrinkles are frequently referred to as ribbing, ridging, tin canning, circumferential ridges, and corrugations. Two main form types of these wrinkles exist. One type, when formed, takes on the diamond pattern or chain link shape. The second type, when formed, occurs as a bump or ridge in the web.

### Sources of CMD Stress

It is unknown whether these circumferential wrinkles are created in the wound roll, if they are from a web defect that manifests itself later after winding, or if both of these cases are true. However, many theories exist about the causes of these wrinkles. Several theories were reported in the Semiannual Technical Review and Industry Advisory Board Meeting Notes [1]. (The following is a brief description of some of the theories given in this reference.)

One theory is that these wrinkles are a result of stresses that exist due to CMD viscoelastic recovery from the extrusion process. Many polymers attempt to recover after extrusion into films. Web tension or draw control may prevent the web roll from contracting in the machine direction but there is no constraint in the cross-machine direction.

Another theory is that these wrinkles are caused by air entrainment. It is often assumed that a perfect web with large stiffness would fly at a constant air film height. However, a less than ideal web is non-uniform in length and typically has small bending stiffness such that air film decays at the edges where the air is escaping or perhaps where the web tension is high due to web length variation. This tension variation can be the source for a CMD stress.

A third theory is that these wrinkles are a result of the winding process. Axial stresses in wound rolls are limited by the magnitude of Poisson's ratio. Poisson's ratio is typically small, but when the wound roll pressures are high and the web blocks together, sizable Poisson's ratios become possible, which can generate significant CMD stresses.

These are just a few examples of the many theories that exist about the causes of circumferential wrinkles in web rolls. Though each theory is different, the common link between many of the theories is a CMD stress (or axial stress) that occurs.

### **Purpose of Project**

Before the theories of the causes of these wrinkles can be studied, the axial stress required to cause such wrinkles must first be investigated. Therefore, the purpose of this study was to measure the critical force required to form a circumferential buckle in a roll of web. Furthermore, in this study the effects of winding conditions on the value of the critical force were investigated. To do this, the critical buckling force was compared to the tension used when winding the roll. The final goal of this project was to determine if any existing mathematical model could be used to predict the critical buckling force of these web rolls, and if not, the goal was to formulate a new model that would predict these critical buckling forces.

## CHAPTER 2

### LITERATURE SURVERY

Several different papers and texts were researched in order to receive a better understanding of the buckling phenomenon that is occurring when a circumferential wrinkle occurs. Several of these papers dealt with the basic buckling of shells, others dealt with the buckling of shells on an elastic foundation, and other papers dealt with web handling in general.

Initial research began with Timoshenko [2]. In this work, Timoshenko solves for the critical stress needed to buckle a uniformly axial compressed cylindrical shell using the energy method. Assuming the shell retains a cylindrical shape until buckling occurs, the total strain energy is the energy of axial compression. When buckling begins, the strain energy of the middle surface in the circumferential direction and bending of the shell must also be considered. Thus, the strain energy of the shell is increased. At the critical value of the load, this increase must equal the work done by the compressive load. In Timoshenko's work, the radial displacement is assumed to take the following sinusoidal shape, and the flexural rigidity is given to be:

$$\text{Equation 2-1} \quad w = -C \sin\left(\frac{m\pi x}{l}\right)$$

$$\text{Equation 2-2} \quad D = \frac{Eh^3}{12(1-\nu^2)}$$

Using the strain energy method, the following equation for the critical stress is found:

$$\text{Equation 2-3} \quad \sigma_{cr} = \frac{N_{cr}}{h} = D \left( \frac{m^2 \pi^2}{hl^2} + \frac{El}{r^2 D m^2 \pi^2} \right)$$

$N_{cr}$  is the force per unit length. In this case the length would be the circumference of the cylinder,  $2\pi r$ . Assuming that there are many waves formed along the length of the cylinder during buckling, considering the critical stress as a continuous function of  $m\pi/l$ , and seeking the half wave number with which the minimum buckling stress  $\sigma_{cr}$  is associated, the equation above becomes:

$$\text{Equation 2-4} \quad \sigma_{cr} = \frac{N_{cr}}{h} = \frac{2}{rh} \sqrt{EDh}$$

By substituting the equation for D, Equation 2-2, into Equation 2-4 the critical stress becomes:

$$\text{Equation 2-5} \quad \sigma_{cr} = \frac{N_{cr}}{h} = \frac{Eh}{r\sqrt{3(1-\nu^2)}}$$

To find the critical force from this equation, the critical stress is multiplied by the area on which the stress is acting,  $2\pi rh$ .

$$\text{Equation 2-6} \quad P_{cr} = \frac{2\pi E h^2}{\sqrt{3(1-\nu^2)}}$$

The length of the half-waves into which the shell buckles is given by the following equation:

$$\text{Equation 2-7} \quad \frac{l}{m} = \pi \sqrt[4]{\frac{r^2 h^2}{12(1-\nu^2)}}$$

Timoshenko also explains how the same critical stress can be found using the equilibrium equation for a cylindrical shell. The equilibrium equation for a cylindrical shell given by Timoshenko is shown below.

$$\text{Equation 2-8} \quad D \frac{d^4 w}{dx^4} + N_x \frac{d^2 w}{dx^2} + Eh \frac{w}{r^2} = 0$$

To solve for the critical stress using this differential equation, substitute the expression for  $w$  (Equation 2-1) into Equation 2-8 and equate to zero the coefficient of  $\sin(m\pi x/l)$ . The result of this method will once again be Equation 2-3, and then, Equation 2-6 can be found again using the same steps as before. An important item to note is that Timoshenko's equation for the buckling of a cylinder assumes that the cylinder takes on a sinusoidal shape when buckled. Therefore, the cylinder is allowed to buckle two ways, inward and outward.

A paper by Allan [3] presented a study of one-way buckling of a beam on an elastic foundation. This paper was of interest because in some web rolls it appears that the core only allows the web shell to buckle outwards. Allen solves the differential equation for a beam using conditions that force the beam to buckle one way. In his experimentation, Allan uses a device to load the ends of a beam that is resting on a foundation of springs. Allan then concludes that depending on the end conditions, which changes the value of  $C$ , the following equation represents one-way buckling of a beam on an elastic foundation:

$$\text{Equation 2-9} \quad P_{cr} = C\sqrt{kEI}$$

Though Allan's paper was of interest due to his coverage of one-way buckling, his paper was limited to the buckling of beams on and elastic foundation and did not cover one-way buckling of shells.

The only paper found that dealt with circumferential wrinkles in rolls of web was a paper by Forrest [4]. In this paper, Forrest develops equations to solve for both transverse and circumferential stresses. The formula takes into consideration entrained air, air gap, and winding tension. In his equation, winding tension affects the radial elastic modulus. The radial elastic modulus was found using a methodology developed by Pfeiffer [5]. In Pfeiffer's equation, the pressure in a roll can be approximated given the properties of the roll and winding conditions, such as web tension. Forrest extended Pfeiffer's equation to include air entrainment, and then gives an equation for a reduced radial elastic modulus as affected by the entrained air. In order to find the critical stress, Forrest uses a finite difference procedure. A program was written which involved dividing the web roll into a number of finite layers. As each successive layer is added to the roll, the circumferential stress, transverse stress, radial elastic modulus, and internal pressures are updated. The initial equilibrium equation for a cylinder that Forrest uses is different from that given by Timoshenko [2]. Neither the source of this differential equation nor a development for it is given in Forrest's paper. Though the equation closely follows Timoshenko [2], the addition of the 3/2 value is not explained. Nonetheless, the important change from Timoshenko's equation is the addition of the foundational stiffness term,  $k$ . Forrest assumes that each layer acts like a cylinder on an elastic foundation. This foundation is made up of the layers underneath the current layer.

Equation 2-10

$$\frac{d^4 w}{dx^4} + \frac{F}{D} \frac{d^2 w}{dx^2} + \frac{3k}{2D} w = 0$$

Since Forrest's initial equation appears sound but lacks verification, a similar methodology will be used in the 'Theoretical Development' Chapter of this paper to develop a buckling equation for a cylinder on an elastic foundation. For this equation, a slightly modified version of the differential equation given by Timoshenko [2] will be used instead of the differential equation used by Forrest [4].

It has been proven that cylinders in axial compression may buckle in one of two modes, one being axisymmetric and one that is not. A book by Allen and Bulson [6] was referred to in order to understand these buckling modes better. The book explains that when buckles occur in the shape of waves in the longitudinal direction, they are commonly called symmetrical or 'ring' buckling. When buckles occur that have waves in both the longitudinal and circumferential direction they are commonly called 'chessboard' buckles. Allen and Bulson then use the energy method to solve for the critical stress needed to cause the 'ring' buckle. Their derivation follows the one presented by Timoshenko [2]. Therefore, the resulting critical force is found to be Equation 2-5. Then, the energy method is used to solve for the critical stress needed to cause the 'chessboard' buckle. In this solution, the following equation is the assumed displacement shape:

$$\text{Equation 2-11} \quad w = -C \sin\left(\frac{m\pi x}{l}\right) * \sin(n\theta)$$

The number of half waves in the longitudinal direction is m. The number of half waves in the circumferential direction is n. Solving for the critical stress gives the following equation:



$$\text{Equation 2-12} \quad \sigma_{cr} = \frac{Eh^2}{12(1-\nu^2)} \left( \frac{(n^2 + (m^2 \pi^2 r^2 / l^2))^2}{r^2 * (m^2 \pi^2 r^2 / l^2)} + \frac{E(m^2 \pi^2 r^2 / l^2)}{(n^2 + (m^2 \pi^2 r^2 / l^2))^2} \right)$$

If  $n$  equals zero, no circumferential waves occur and the above equation simplifies to Equation 2-5. Thus, Allen and Bulson explain that the critical stress is the same for ring buckling and chessboard buckling if  $m^2$  is a large number and is independent of the length. Therefore, the critical force found in Timoshenko [2] can be used for either buckling shape when this assumption is made. For web rolls, the internal pressure caused by winding the web onto the surface of a winding roll acts to prevent the ‘chessboard’ wrinkles from occurring and allows only for the ring modes. Sometimes the ‘chessboard’ wrinkles form in the outside lap of a wound roll where the tail of the web was not secured to the wound roll under tension.

For basic engineering equations, equations commonly used in web handling, and to gain some further knowledge on the buckling of shells and plates, several other works were referenced as needed. For the basic equations related to stress, strain, force, and material properties, Shigley [7] was used. In particular, the equation given by Shigley for the hoop stress of a thin walled cylinder was used.

$$\text{Equation 2-13} \quad \sigma_{t,av} = \frac{pd}{2h}$$

This equation was also found in Budynas [8]. However, Budynas was primarily used for a related equation, which gives the deformation for a thin walled cylinder under pressure.

This equation is given below:

$$\text{Equation 2-14} \quad u_r = (2 - \nu) \frac{pr^2}{2Eh}$$

Both of these equations were used for calculating the frictional effects of the core.

To determine the pressure and radial elastic modulus, which vary as a function of radius in a wound roll, a winding program was used. For this winding program the material properties,  $K_1$  and  $K_2$ , of the web material were found using a method presented by Pfeiffer [5]. In his work, Pfeiffer developed the following equation that can be used to determine the relation between pressure and strain in a stack of web material: (The description of a stack test and the use of this equation can be found in the 'Experimental Procedure and Setup' Chapter. This is also the equation mentioned earlier that was used by Forrest [4] to help determine the pressure and radial elastic modulus of each layer within the roll.)

**Equation 2-15**       $p = K_1(e^{K_2\epsilon} - 1)$

# CHAPTER 3

## THEORETICAL DEVELOPMENT

### **Introduction to Models**

Due to the complexity of a roll of web, five different models were developed in order to find the analytical model which best described a roll. Two models were developed that used Timoshenko's model for a cylindrical shell. One model was developed using a cylindrical shell on an elastic foundation. Another model was developed which consisted of a cylindrical shell on a rigid surface with a stabilizing external pressure. The final model also used *Timoshenko's model* for a cylindrical shell but took into account frictional effects due to the testing apparatus.

### **Axially Compressed Cylindrical Shell Models**

Two models were initially developed that used Timoshenko's buckling equation, Equation 2-6. Model #1 assumes that the web roll acts like one large cylinder. In this model, the roll dimensions are used for the inputs into Timoshenko's equation, where the thickness of the cylinder equals the thickness of the roll. Model #2 assumes that the roll acts like multiple cylinders. In this model, Timoshenko's equation is used to find the buckling force for each cylinder, where the thickness of the cylinder equals the thickness of the web. To find the buckling load for the roll, the individual buckling loads are summed together. The only concern with these models is that they do not consider the winding tension at which the roll is wound. Since winding tension affects values within

the roll such as pressure and radial elastic modulus, three other models were developed which included tension affects.

### Shell on Elastic Foundation Model

So that tension would factor into the buckling equation, a modified version of Equation 2-8 was developed. In this model, each layer of web is assumed to behave like a cylindrical shell on an elastic foundation. When a cylinder is said to be on an elastic foundation, the terminology is describing a case in which the inside of the cylinder or core of the cylinder is made up of an elastic material. In the case of the web roll model, it is assumed that for each layer of web, the layers of web under it act like an elastic foundation. A diagram of the model can be seen in Figure 3-1.

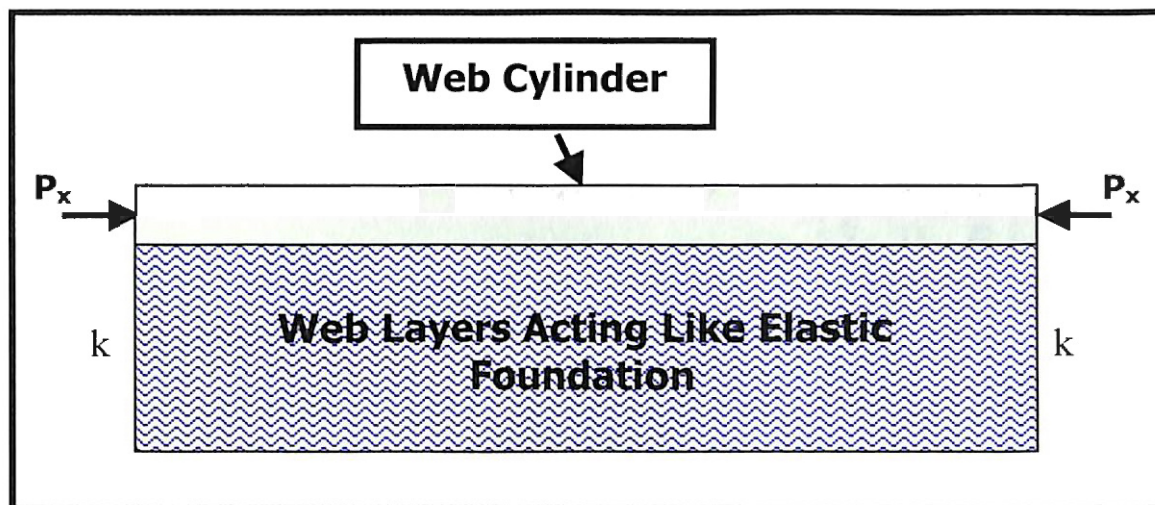


Figure 3-1: Diagram of Cylindrical Shell on an Elastic Foundation Model.

In order to develop an analytical solution to this model, the following modified version of the differential equation given by Timoshenko [2], Equation 2-8, will be used:

$$\text{Equation 3-1} \quad D \frac{d^4 w}{dx^4} + N_x \frac{d^2 w}{dx^2} + \left( \frac{Eh}{r^2} + k \right) w = 0$$

In this differential equation,  $k \cdot w$  was added in order to represent the effects of an elastic foundation. This  $k$  value is the foundational stiffness. Using the second method described by Timoshenko [2], the assumed radial displacement, Equation 2-1, is substituted into Equation 3-1. Canceling like terms and solving the equation gives the critical force (per unit length):

$$\text{Equation 3-2} \quad N_{cr} = D \left( \frac{m\pi}{h} \right)^2 + \left( \frac{Eh}{r^2} + k \right) \left( \frac{l}{m\pi} \right)^2$$

Assuming there are many waves formed during buckling, considering  $N$  as a continuous function of  $m\pi/l$ , and determining the value of  $m$  which yields the minimum value of the axial load per unit of circumferential length required to buckle the cylinder, the equation becomes:

$$\text{Equation 3-3} \quad N_{cr} = D \sqrt{\frac{Eh}{r^2 D} + \frac{k}{D}} + \left( \frac{Eh}{r^2} + k \right) \left( \frac{1}{\sqrt{\frac{Eh}{r^2 D} + \frac{k}{D}}} \right)$$

Simplifying the equation above results in the following equation:

$$\text{Equation 3-4} \quad N_{cr} = \frac{2\sqrt{D(Eh + r^2 k)}}{r}$$

To find the critical force, the equation above is multiplied by the circumference of the shell,  $2\pi r$ .

$$\text{Equation 3-5} \quad P_{cr} = 4\pi \sqrt{D(Eh + r^2 k)}$$

By substituting the value of D, Equation 2-2, into the above equation, it becomes the following: (Note that if k is zero the equation reduces to the critical force found using Timoshenko's method, Equation 2-6.)

$$\text{Equation 3-6} \quad P_{cr} = 2\pi \sqrt{\frac{E^2 h^4 + E h^3 r^2 k}{3(1-\nu^2)}}$$

To employ these expressions requires the foundational stiffness, k, to be found. First, the radial elastic modulus is found using a winding program. In this program, the values of  $K_1$  and  $K_2$  are entered as well as the winding parameters such as inner diameter, outer diameter, material properties, and winding tension. ( $K_1$  and  $K_2$  are found using Equation 2-15 after curve fitting stress versus strain data from a stack test.) The radial elastic modulus is then used to find the foundational stiffness using the following equation:

$$\text{Equation 3-7} \quad pA = \frac{E_r A}{t} \Delta$$

Canceling the A on both sides and rearranging the equation leads to the following equation:

$$\text{Equation 3-8} \quad k = \frac{p}{\Delta} = \frac{E_r}{t}$$

Therefore, k can be found by dividing the radial elastic modulus by the thickness of the part of the shell acting like an elastic foundation. With k, the critical force can be solved for using Equation 3-6.

To find the critical force using the elastic foundation model, the following method was used. The critical force was found for each layer or cylinder of web starting with the first layer. For each layer that was added, a winding program was used to calculate the

radial elastic modulus. With this value and the thickness of the layers below the current layer, a foundational stiffness was found for the current layer using Equation 3-8. Then, the critical force for that layer was found through input of the following values into Equation 3-6: the current foundational stiffness, the shell thickness, the elastic modulus, and the radius for that layer. This process was repeated for every layer, and then the critical forces for each layer were summed to find the critical force for the entire web roll.

As will be shown later in the 'Results and Discussion' Chapter of this paper, the elastic foundation model gave results that were much greater than the experimental results. Therefore, more approaches were formulated in order to better model the true buckling situation.

#### **Shell on Rigid Core with External Pressure Model**

Some problems with the above theoretical solution is that it assumes that the shell buckles in two directions and that the elastic foundation is assumed to affect the buckling of the shell in two directions (much like an attached spring.) However, in the actual case, as the shell begins to buckle outwards it should no longer be affected by the foundation. Furthermore, the shell only buckles in one direction in many of the actual cases. Therefore, a new model, Model #4, was developed which considered these problems. In this model, a cylindrical shell was made which rested on a rigid surface. Then, a pressure was added to the outside of the shell. This pressure, like the radial elastic modulus in Model #3, was found using WINDER, a winding software program. The shell was then compressed axially. Due to the core on the inside, the pressure would act to stabilize the shell. Hence, higher pressures would result in higher critical buckling forces. In

addition, the rigid core would only allow the cylinder to buckle outwards. A force diagram and configuration of the model can be seen in Figure 3-2.

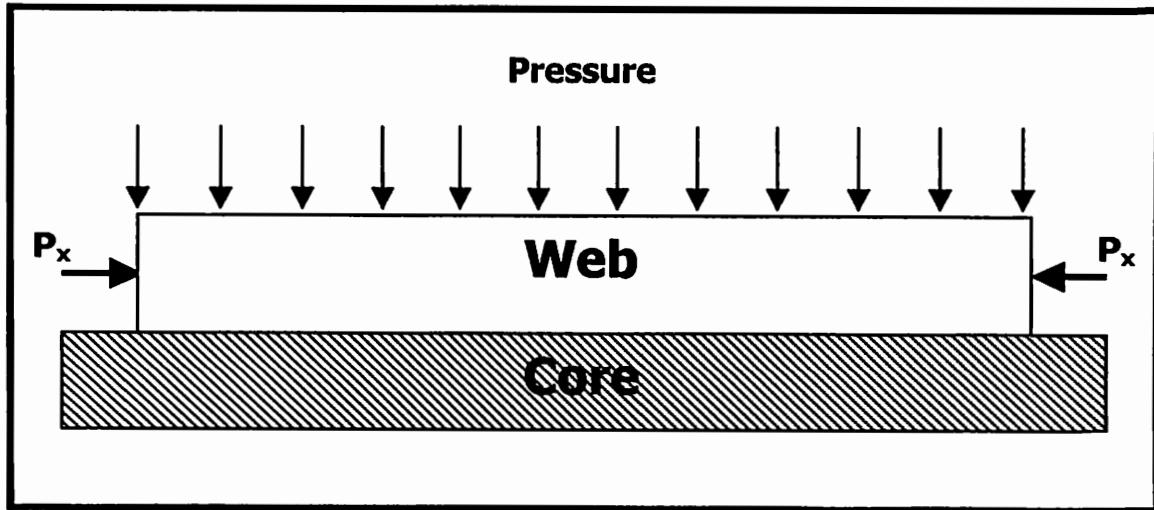


**Figure 3-2: Model of Cylinder on Rigid Core with Pressure.**

Due to the complexity of this model several computer programs that used finite element methods were employed: ABAQUS, Pro/MECHANICA, COSMOS, and CADRE. Though several attempts were made with each program to model the problem, all attempts failed. In the end, either each program had limitations that would not allow the problem to be set up correctly, or the program could not correctly run the problem once it was set up. However, as will be seen in the ‘Results and Discussion’ chapter, this model was not needed in order to explain the experimental results.

### **Axial Compression with Apparatus Effects Model**

As mentioned above, Model #3 did not give good results and Model #4 could not be solved for correctly using FEM programs. Therefore, a new method, Model #5 was developed. Though Timoshenko’s model of an axially compressed cylinder does not include tension effects, the resulting high-pressures at the center of a roll due to winding could affect the specially designed core, which was used to test the rolls. (A close-up of



this core can be seen below in Figure 3-3.) Though the core was designed to have enough tolerance between the sides of teeth to limit frictional forces, large pressures on the surface of the core ( $p$  in Figure 3-3) due to winding may cause the tolerance to vanish. If this occurs, the resulting stress within the core,  $\sigma_t$ , owing to the pressure in the roll would be high enough to create a large frictional force between the teeth.

To test this model, a winding program was used to find the pressure at the core for rolls made at each tension setting. Using this pressure, Equation 2-13 was used to calculate the resulting hoop stress within the core. The area of contact between the sides of the teeth was then found using Equation 3-9. (As can be seen in Figure 3-3:  $L_c$  is the length of the contact zone;  $W_c$  is the width of the contact zone; and  $A_c$  is the area of the contact zone.)

$$\text{Equation 3-9} \quad A_c = L_c \cdot W_c$$

Using the coefficient of friction for steel on steel, the hoop stress within the core, and the contact area between the sides of the teeth, the resulting frictional force between the teeth was found using Equation 3-10 where  $\mu$  is the coefficient of friction:

$$\text{Equation 3-10} \quad F_{fric} = \mu \sigma_t A_c$$

Since there were six teeth on each side of the core and two sides to each tooth, twelve zones of contact existed when the core was assembled. To find the total frictional force for the core, Equation 3-10 was multiplied by twelve. The total frictional force for the core was then added to the critical force found using Timoshenko's equation, Model #2. This combination of forces was then compared to the experimental results. In order for

this model to work, the assumption was made that the pressure at the core is high enough at each tension level to close the space between the sides of the teeth.

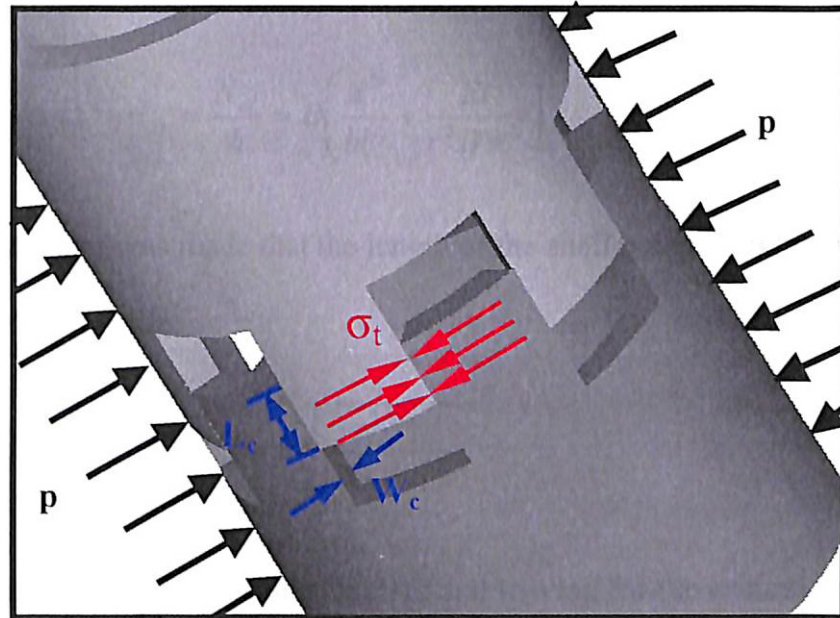


Figure 3-3: Toothed Core with Dimensions of Contact Area of Teeth Labeled

With this toothed core seen above, the web roll is forced to buckle outwards only. However, if the critical buckling force is found using Timoshenko's equation for the buckling of cylinders, the assumption is made that the cylinder buckles two ways, inwards and outwards. Therefore, for Model #5 to model the experimental data correctly it must first be shown that one-way buckling and two-way buckling result in the same critical buckling force.

If a single one-way wrinkle occurs during buckling, it can be assumed that this one-way buckle is simply half of a two-way buckle. This was done computationally by using a half wave number of one in Equation 2-1. This resulted in the following equation:

Equation 3-11 
$$w = -C \sin\left(\frac{\pi x}{l}\right)$$

Following Timoshenko's example given in Chapter 2, the critical force was then found to be:

$$\text{Equation 3-12} \quad \sigma_{cr} = \frac{N_{cr}}{h} = D \left( \frac{\pi^2}{hl^2} + \frac{El}{r^2 D \pi^2} \right)$$

Then, the assumption was made that the length of the shell being buckled would be equal to the length of the buckle:

$$\text{Equation 3-13} \quad l = \pi \sqrt[4]{\frac{r^2 h^2}{12(1-\nu^2)}}$$

By substituting this length into Equation 3-12 and solving for the critical force, the following critical force equation was found:

$$\text{Equation 3-14} \quad P_{cr} = \frac{2\pi E h^2}{\sqrt{3(1-\nu^2)}}$$

This is the same critical force found by Timoshenko when assuming two-way buckling, Equation 2-6. Hence, if these assumptions are made, Timoshenko's buckling equation, Equation 2-6, can be used to calculate the critical force for the one-way buckles that occur in wound web rolls. These assumptions can be checked experimentally by measuring the wavelength of the one-way buckle.

## **CHAPTER 4**

### **EXPERIMENTAL SETUP AND PROCEDURE**

#### **Machine Setup**

An existing WHRC winding station was used to wind the rolls. The machine consisted of an unwind roll, load cell, winding roll, and intermediate transport rollers. The tension in the web was maintained by a Magpowr dual magnetic hysteresis brake, which was controlled by a Magpowr Digitrac controller. The controller monitored the tension in the web using a Magpowr 50 lb load cell. The speed of the web was controlled by a Reliance Electric Speed Controller and Reliance electric AC motor, which was coupled to the winding roll. A labeled setup of the machine can be seen in Figure 4-1.

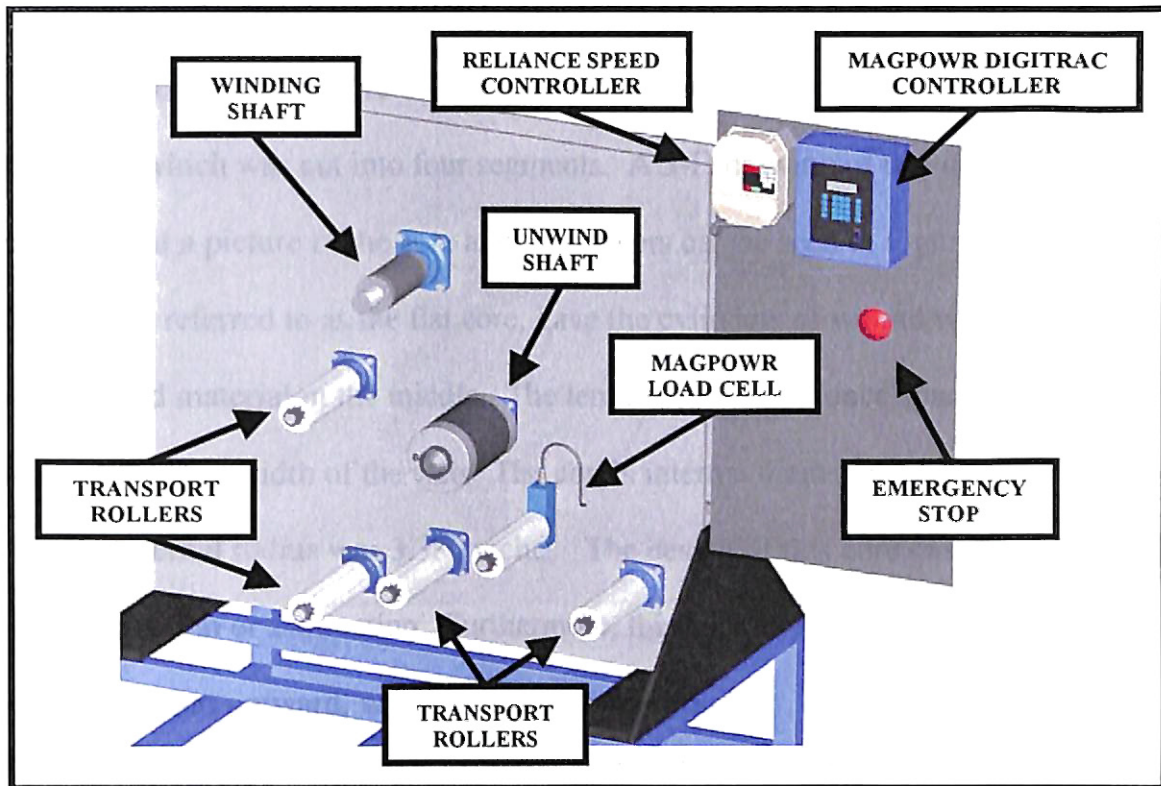


Figure 4-1: Labeled Setup of Winding Machine

## Core Design

Specially designed cores were made so that wound rolls of web could be crushed in the Instron. Though two different cores were made, both of them had to meet these two requirements: each had to mount onto the winding shaft of the web machine and each had to have a gap in the middle which would allow the roll of web to be axially crushed in the Instron without interference from the core. To meet these requirements, the cores were designed with removable spacers. These spacers allowed for the two end pieces of the core to be correctly mounted into the winding machine and maintained the desired core length. Furthermore, these spacers could be removed once a roll of web was wound, which left a gap in the middle of the core. This gap allowed the cylinder of wound web to be compressed in the Instron. The dimensions for each roll can be found in Table 4-1.

### *Flat Core Specifications*

The first designed core consisted of two main parts: two end pieces and a removal centerpiece, which was cut into four segments. A 3-D drawing of this core can be seen in Figure 4-2 and a picture of the core and the spacers can be seen in Figure 4-3. This core, which will be referred to as the flat core, gave the cylinders of wound web .5 inches of non-supported material in the middle. The length of the core, once spaced, was 6 inches, which matches the width of the web. The core's internal diameter was 2.95 inches and the core's external radius was 3.380 inches. The design of this core gave no restraint in the theta-direction or z-direction. Furthermore, this core allowed for two-way buckling to occur, inward and outward, when the roll was compressed.

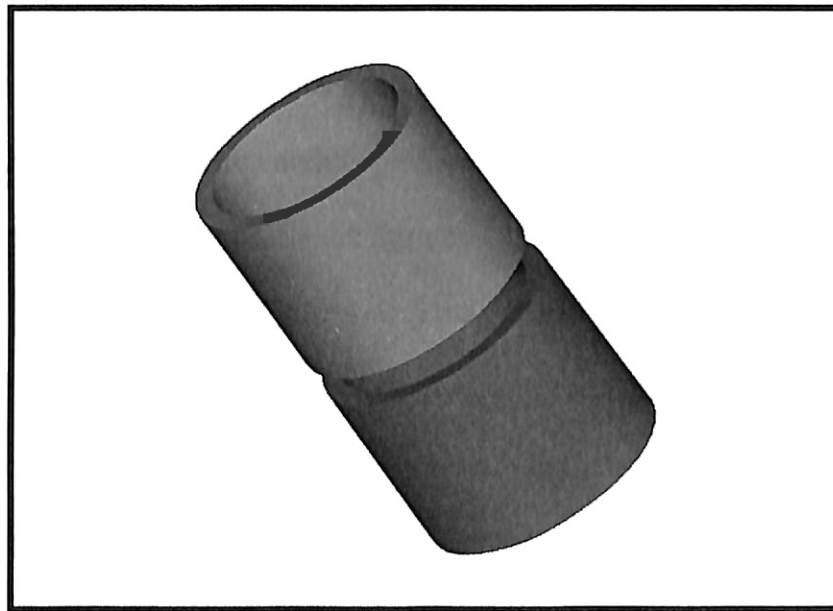


**Figure 4-2: 3-D Model of Flat Core**

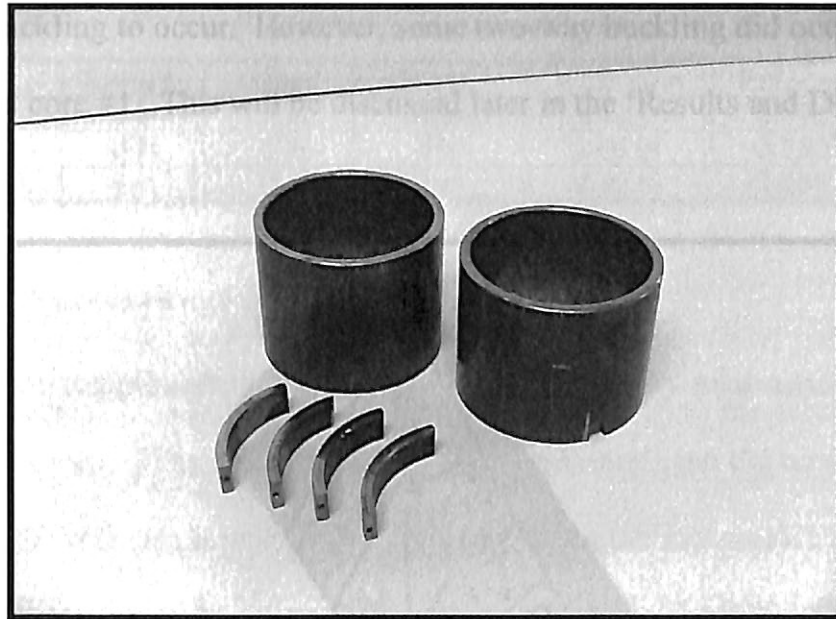


**Figure 4-3: Photograph of Flat Core and Spacers**

### *Toothed Core Specifications*

The second core designed also consisted of two main parts: two end pieces with six evenly spaced teeth and three middle pieces used as spacers. As can be seen in Figure 4-4, the teeth of the two end pieces were designed to interlock. A picture of the actual core and spacers can be seen in Figure 4-5. Two versions of the toothed core were made. The first version had a gap of .5 inches, which matches the gap size of the flat core. This .5 inches gapped core will be referred to as toothed core #1. The second version of the toothed core had a gap of only .15 inches in order to minimize the effects of the gap on the buckling criteria. This core will be referred to as toothed core #2. The length of both cores, once spaced, was 6 inches. The internal diameters of the both cores were 2.95 inches. Toothed core #1 had an external diameter of 3.380 inches, and toothed core #2 had an external diameter of 3.365 inches. The teeth of both toothed cores were 1 inch long. Due to these teeth, both cores allowed for movement in the (axial) z-direction, but gave restraint in the theta direction. Furthermore, these cores were designed to not allow

for two-way buckling to occur. However, some two-way buckling did occur in the large gaps of toothed core #1. This will be discussed later in the ‘Results and Discussion’ chapter.

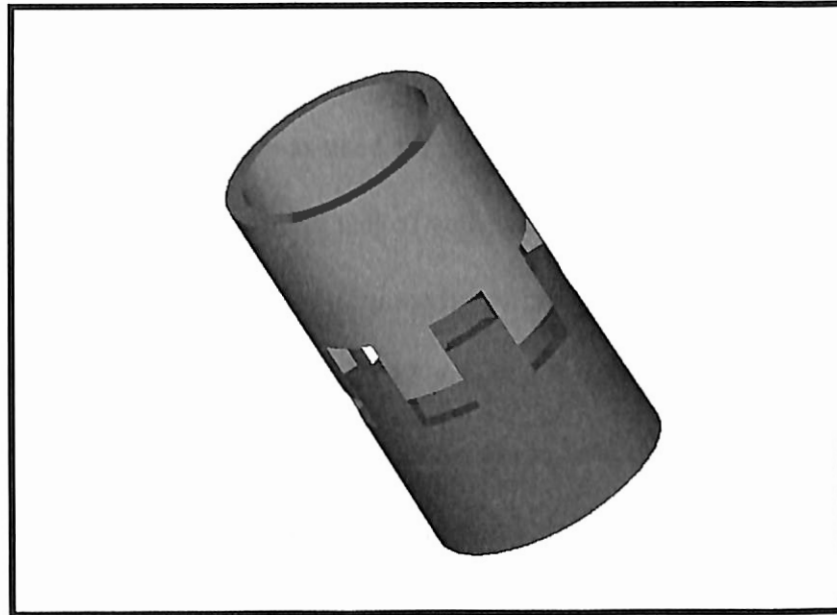


**Figure 4-4: 3-D Model of Toothed Core**

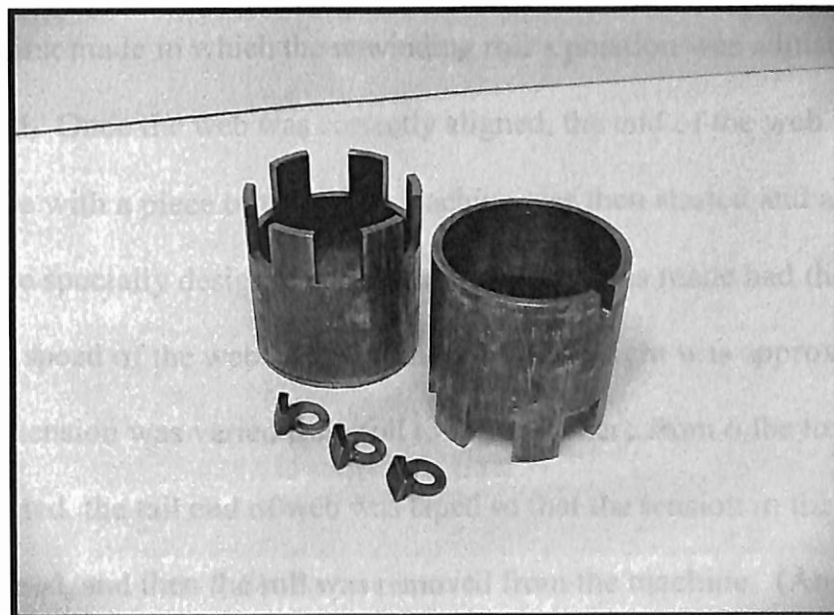


**Figure 4-5: Photograph of Toothed Core and Spacers**



**Table 4-1: Dimensions of Cores**

<b>Core Type</b>	<b>Length</b>	<b>Gap</b>	<b>Tooth l</b>	<b>Internal d</b>	<b>External d</b>	<b>Core h</b>
Flat Core	6 in	.5 in	none	2.95 in	3.380 in	.215 in
Toothed Core #1	6 in	.5 in	1 in	2.95 in	3.380 in	.215 in
Toothed Core #2	6 in	.15 in	1 in	2.95 in	3.365 in	.2075 in

## **Experimental Procedure**

The following procedure was used for all of the primary tests conducted with the flat and toothed cores. First, a wound roll of web was loaded onto the unwind shaft of the winder. Then, the roll was secured into place by inflating the expandable shaft. The material that was used for all tests was a 142-gauge polyester film (.00142 inches thick.) Next, the spacers were taped into place, and one of the specially designed cores was assembled. The core was then loaded onto the wind shaft and secured into place by a nut on the end of the wind shaft. The web was then threaded through the machine as shown in Figure 4-6. In order to align the unwinding web with the winding core, several attempts were first made in which the unwinding roll's position was adjusted until properly aligned. Once the web was correctly aligned, the end of the web was attached to the winding core with a piece of tape. The machine was then started and a roll of web was made on the specially designed cores. Each roll that was made had the following parameters: the speed of the web was 50 ft/min, the pile height was approximately .25 inches, and the tension was varied from roll to roll anywhere from 6 lbs to 26lbs. Once a roll was completed, the tail end of web was taped so that the tension in the web was closely maintained, and then the roll was removed from the machine. (Any roll that had too much drift in edge position in the cross-machine direction was thrown out; only rolls with nice aligned ends were kept for testing.) Next, the spacers were removed from the roll through the center of the core. Then, the final diameter of the core was measured

using calipers. Finally, the roll was placed between the platens of the Instron, where the roll was compressed past the point of buckling. The Instron compressed the roll axially in velocity control. The output from the Instron was axial deformation and force. This data was used to establish charts of force versus deformation. The charts were then used to determine at what load the test deviated from linear elastic behavior. Typically, an inflection or a change in slope in the chart was used to determine the onset of buckling.

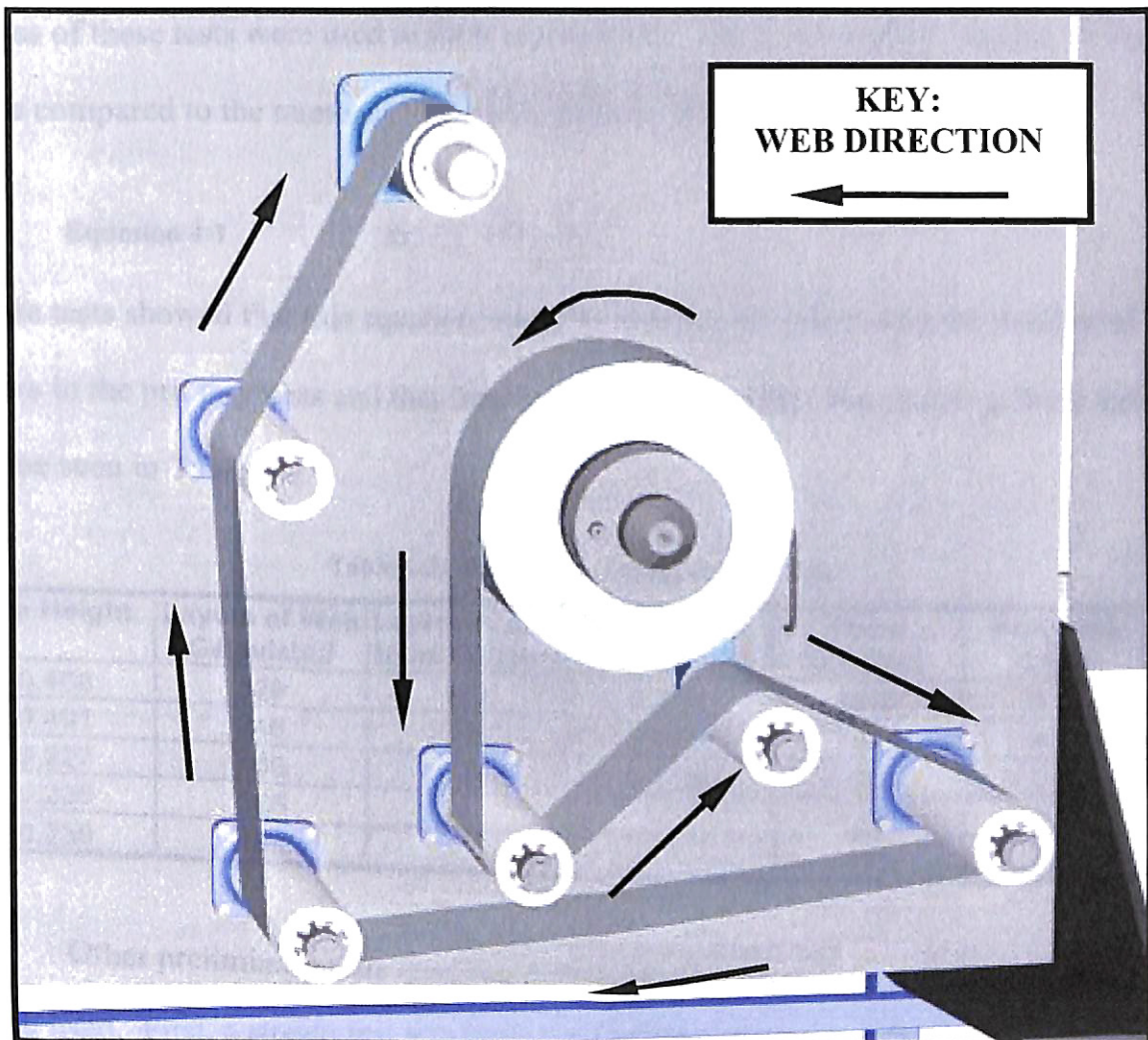


Figure 4-6: Setup of Web Path

## Preliminary Tests

Several preliminary tests were run in an effort to eliminate problems in the procedure and to insure the repeatability of the experimentation. First, five rolls were wound on the flat core at 9 lbs of tension, at a speed of 50 ft/min, and a pile height of either approximately .25 or .5 inches. Besides measuring the buckling force of these rolls, the numbers of layers of three of these rolls were counted by hand. The buckling forces of these tests were used to show repeatability. The hand-counted number of layers were compared to the number of layers found using the following equation:

$$\text{Equation 4-1} \quad \text{layers} = \frac{r_o - r_i}{h}$$

These tests showed that this equation would be accurate for calculating the number of layers in the primary tests and that these tests were repeatable. Results from these tests can be seen in Table 4-2.

Table 4-2: Results from Preliminary Tests

Pile Height	Layers of Web Calculated	Layers of Web Hand Counted	Percent Error (Web Layers)	Force (Instron)	Force per Layer
0.468	329	328	0.37%	1380	4.19
0.491	346	344	0.52%	1400	4.05
0.227	160	161	0.93%	620	3.89
0.235	165			650	3.93
0.239	168			680	4.04

Other preliminary tests were run to determine the properties of the web material being used. First, a stretch test was performed on the material in order to calculate the elastic modulus of the material. To perform this test, 50 ft of material was rolled out onto a long stretch of floor. This test was run in lieu of the ASTM D882 standard for determining the modulus of plastic films. The stretch test is superior in that specimen

end effects are minimized through the use of a long sample. One end of the material was secured to the floor using tape and weights. The other end was connected to a force gauge. The material was then loaded from 0 lbs to 60 lbs, and the resulting elongation was marked on a piece of paper for every 5 lb increments of force. Using this data, a stress versus strain graph was plotted as seen in Figure 4-7. The slope of this graph, which is the elastic modulus of the material, was found to be 718054 psi.

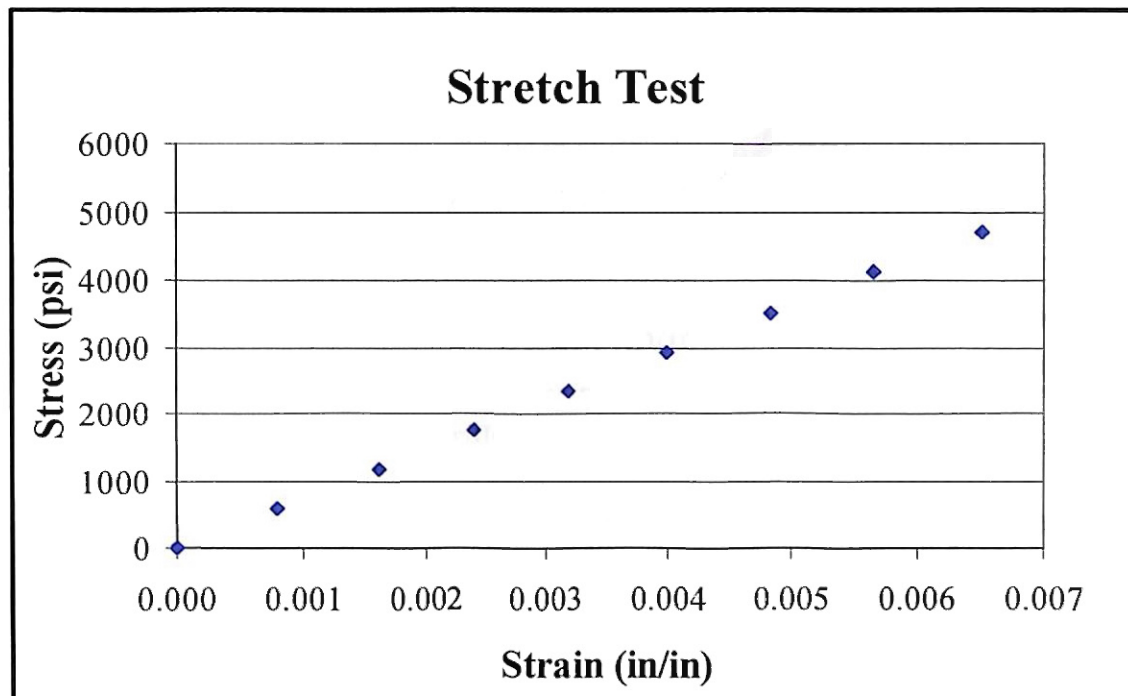


Figure 4-7: Plot of Stretch Test Performed on 142 Gauge Polyester Film

Another preliminary test that was performed was a stack test. This test was used to find the  $K_1$  and  $K_2$  values for the equation developed by Pfeiffer, Equation 2-15. To conduct this test, a 1-inch thick stack of web material was cut off the roll. This stack of material was then compressed in the Instron. The output from the Instron was in the form of load and distance. This data was converted to pressure and strain. The  $K_1$  and  $K_2$  parameters were then determined using a least squares error routine. The values for  $K_1$

and  $K_2$  were found to be .4514 and 201.178. A comparison of Pfeiffer's equation to the experimental pressure versus strain curve can be seen in Figure 4-8.

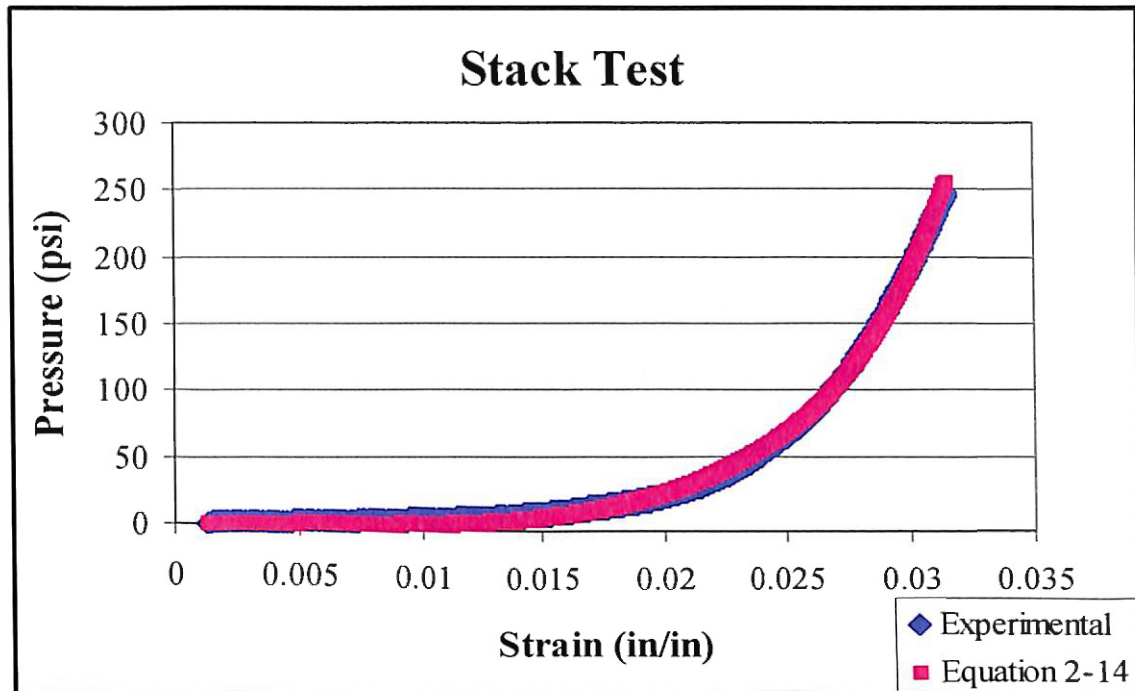


Figure 4-8: Plot of Pfeiffer's Equation and Results of Stack Test

With the  $K_1$  and  $K_2$  values determined, the pressures and radial elastic modulus could now be found using WINDER, a proprietary winding software package created by the WHRC. In the table below, the maximum internal pressure and the corresponding radial elastic modulus found for each winding tension setting used for testing toothed core #2 are shown. (These values are being provided since they will be used in the 'Results and Discussion' chapter to compare experimental results to values found using models #3 and #5.) These computations relied upon the core dimensions listed in Table 4-1 and the material properties found in Table 4-5. The pile height of the web is assumed to be .251 inches or 177 layers. Pile height is the measure of the thickness of web material wound on a roll. It can be calculated by subtracting the final web roll radius by the external radius of the core.

**Table 4-3: Radial Elastic Modulus and Pressures Found Using a Winding Program**

<b>Winding Tension (lb)</b>	12	14	16	18	20	22	24	26
<b>E<sub>r</sub> (psi)</b>	36242	43124	50022	56932	63850	70774	77702	84634
<b>Pressure (psi)</b>	180	214	248	283	317	352	386	421

### Primary Tests

The purpose of the primary tests was to measure the critical force needed to buckle of roll of material and to see if the winding tension affected the resulting critical force. To accomplish this, the sets of tests listed in Table 4-4 were performed using the procedure mentioned above in the ‘Experimental Procedure’ section of this chapter. Each of these sets consisted of eight individual tests in which tension was varied in increments of 2 lbs. The core type and tension range used for each set of tests is described in the following table:

**Table 4-4: List of Primary Tests Performed**

<b>CORE USED</b>	<b>WINDING TENSIONS Of Sets (lb)</b>	<b># OF SETS CONDUCTED</b>
Flat	6, 8, 10, 12, 14, 16, 18, 20	2
Toothed #1	6, 8, 10, 12, 14, 16, 18, 20	2
Toothed #2	6, 8, 10, 12, 14, 16, 18, 20	1
Toothed #2	12, 14, 16, 18, 20, 22, 24, 26	3

The data collected from these experiments was then compared to the five models developed earlier in the ‘Theoretical Development’ chapter. (The results from these tests and the comparison of these tests to the solution models are described in the ‘Results and Discussion’ chapter.) Any core dimensions used in calculations can be found in Table 4-1. Material properties used in these calculations can be found in Table 4-5.

**Table 4-5: List of Material Properties**

<b>Material Properties</b>	<b>Value</b>
Elastic Modulus MD	718054 psi
Poisson's Ratio	.3
Thickness	.00142 in
Width	6 in
K <sub>1</sub>	.4514
K <sub>2</sub>	201.178

## CHAPTER 5

### RESULTS AND DISCUSSION

The purpose of this project was to develop a model that accurately described the circumferential wrinkles in web rolls; the experimental data was compared to the five models discussed earlier Chapter 3. A list of these solution models can be found in Table 5-1. The results and discussion of the flat core will be presented first. Then, the results and discussion of the toothed cores will be presented.

**Table 5-1: Descriptions of Theoretical Models**

MODEL #	EQUATION	DESCRIPTION
1	Equation 2-6	Timoshenko's equation for the buckling of a cylinder is used to calculate the buckling force of the web roll assuming that it acts like one solid cylinder.
2	Equation 2-6	Timoshenko's equation for the buckling of a cylinder is used to calculate the buckling force of each layer of web as if the roll is made up of multiple cylinders. The critical buckling force for the roll is found by summing the buckling forces found for each layer.
3	Equation 3-6	This model uses the developed buckling equation for a cylinder on an elastic foundation. In this model, the procedure used by Forrest [4] is followed. The critical force for each layer is found by assuming the layers underneath it act like an elastic foundation. For each layer, the radial elastic modulus is found and used to calculate the foundational stiffness, k.
4	FEM	Several FEM programs were used to create a cylinder on a rigid foundation with external pressures acting on it. The critical force for each layer is found, and then the values are summed to find the critical buckling force for the web roll. This model will not be used for comparison since all FEM codes failed to model the situation appropriately.
5	Equation 2-6	This model uses the model described in Model #2, but includes the frictional force of the teeth, which results from the pressures at the center of the roll. This frictional force is calculated using the parameters of the roll, and then it is added to the critical force found using Equation 2-6.



## Flat Core Analysis and Discussion

The flat core allowed for two-way buckling because the web layers were unsupported in the region where the buckling occurred. Furthermore, the core did not prevent the roll from twisting along the axis of the cylinder when being crushed. It can be seen in Figure 5-1 that the buckles took on the chain link appearance. This buckling shape occurred for all tests conducted using the flat core. As mentioned earlier in the ‘Theoretical Development’ chapter, these buckles are also known as ‘chessboard’ buckles.

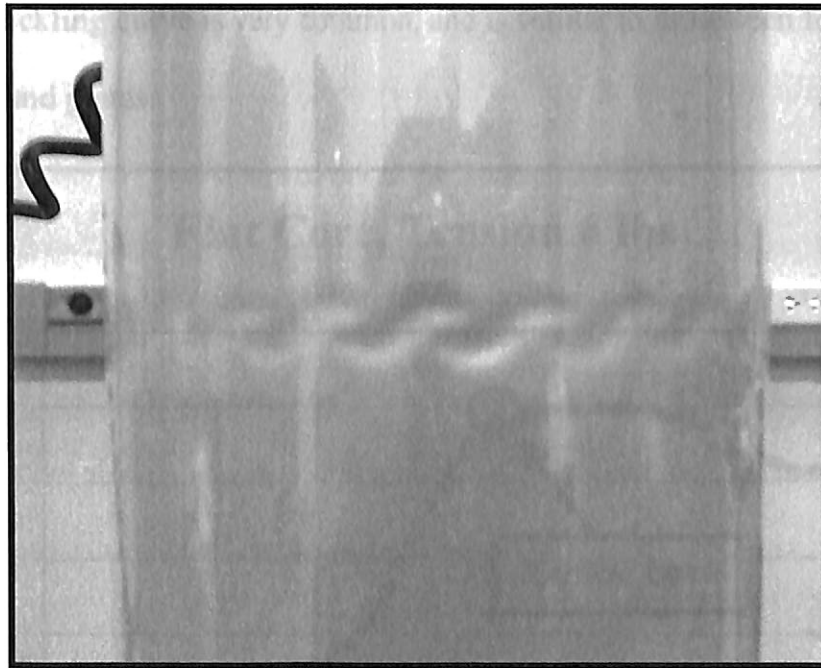


**Figure 5-1: Buckling Shape Resulting from Flat Core Tests**

As mentioned in the ‘Experimental Setup and Procedure’ chapter, two sets of eight tests were conducted on the flat core. The only input that was varied from test to test was the winding tension (6 lbs to 20 lbs.) Since the external diameter changed slightly from test to test, the final buckling force was divided by the number of layers in that roll in order to yield a buckling force per layer value. This value allowed for tests at

different tensions to be compared to each other without the diameter of the roll affecting the data. Likewise, it allowed for tests run at the same tension to be compared to each other without having effects from the slight differences in roll diameters. This procedure was deemed acceptable because the buckling models (Equation 2-6, for instance) do not show a dependence on radius.

To find the critical force at which a roll buckles, the point at which deviation from linear behavior occurs was recorded. As can be seen in the example case shown in Figure 5-2, the roll cannot support higher loads as the roll continues to be compressed. This type of buckling curve is very common, and is similar to those seen for axially loaded beams and plates.

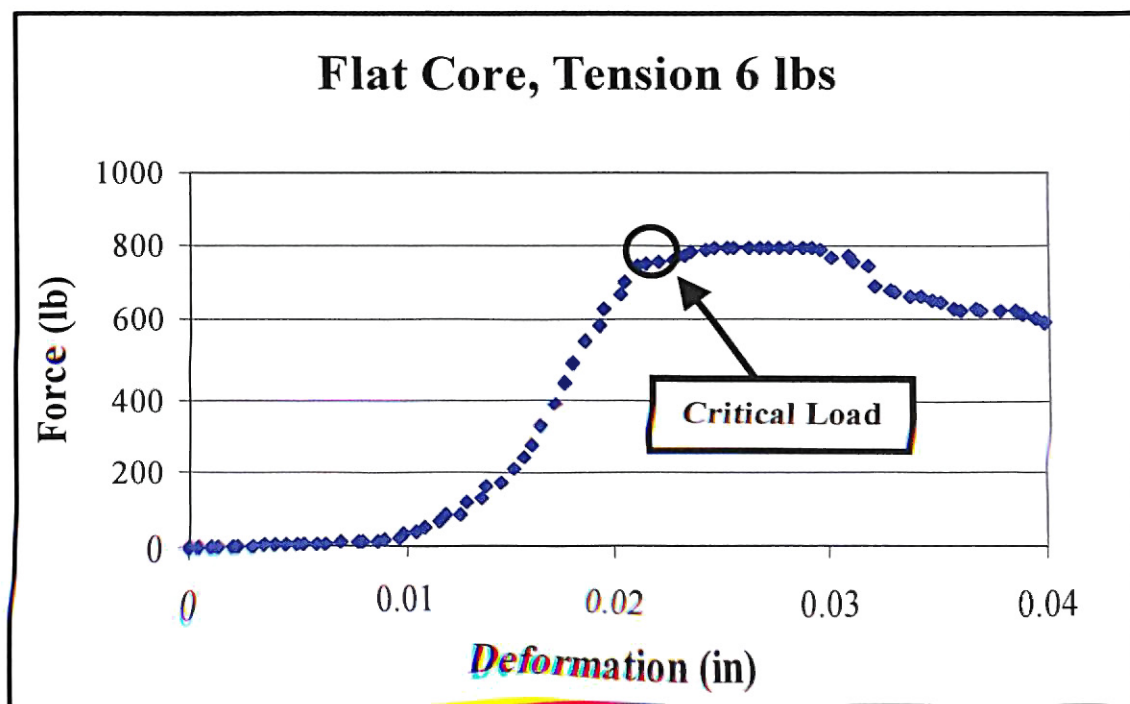


Figure 5-2: Example Buckling Curve for Flat Core

Every test conducted using the flat core resulted in a similar buckling curve. Table 5-2 shows the critical buckling force found for each roll tested in the two sets of tests conducted using the flat core. As mentioned at the beginning of this chapter, the

results are shown as force per layer in order to compare the two sets of tests without worrying about the slight differences in roll diameter. The average critical force for each tension will be used to compare the experimental values to the theoretical models. It should also be noted that the data found using the flat core is very repeatable. The two tests virtually gave identical results.

**Table 5-2: Critical Forces Found for Tests Conducted on the Flat Core**

<b>Winding Tension</b>	<b>6 lbs</b>	<b>8 lbs</b>	<b>10 lbs</b>	<b>12 lbs</b>	<b>14 lbs</b>	<b>16 lbs</b>	<b>18lbs</b>	<b>20 lbs</b>
<b>Set 1 <math>N_{cr}/\text{layer}</math></b>	4.70	4.73	3.65	4.10	3.94	4.33	4.56	5.71
<b>Set 2 <math>N_{cr}/\text{layer}</math></b>	4.80	4.66	3.54	4.10	3.89	4.19	4.57	5.71
<b>Avg. <math>N_{cr}/\text{layer}</math></b>	4.75	4.70	3.60	4.10	3.91	4.26	4.56	5.71

Since the flat core allowed for two-way buckling, much as Timoshenko assumes in his theory, Model #1 was used first for comparison. Using Equation 2-6, the material properties found in Table 4-5 and the averaged pile height of .295 inches, the critical force was calculated for the roll. Then, the critical force per layer was found by dividing the critical force for the roll by the number of layers in the roll. Using the average pile height from the experimental tests and Equation 4-1, the number of layers was found to be 208. The comparison of Model #1 to the experimental data can be found in Figure 5-3.

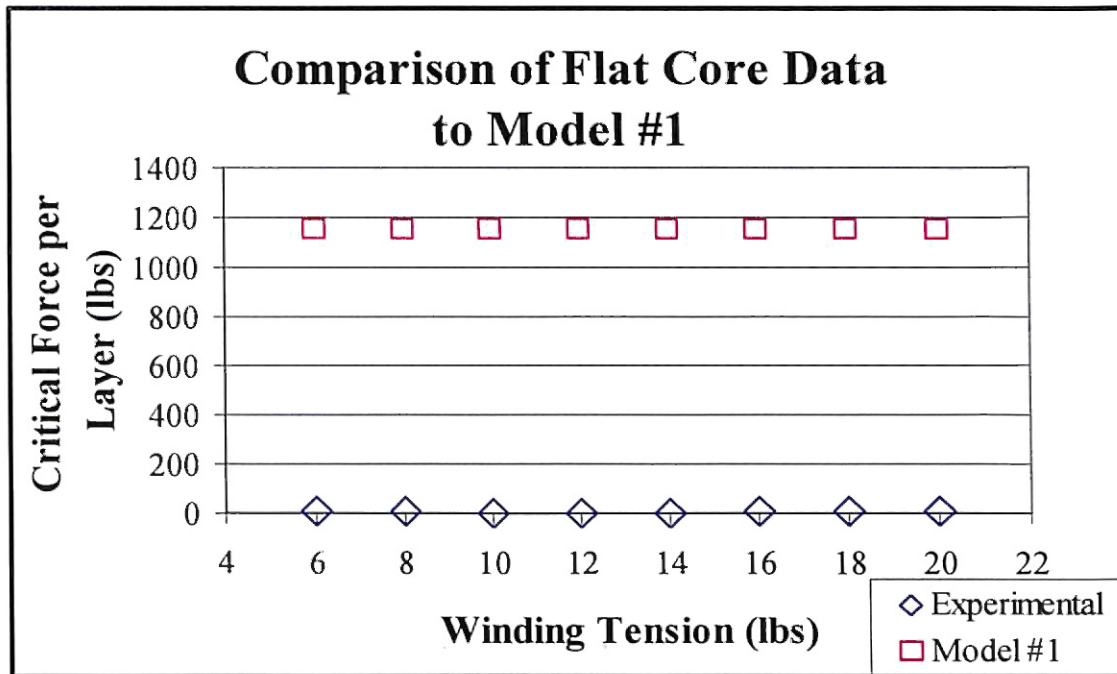


**Figure 5-3: Comparison of Experimental Flat Core Data to Model #1**

From the graph, it can be seen that Model #1 results in values much higher than the experimental data. This means that the web roll should not be modeled as one solid cylinder. Therefore, the experimental data was then compared to Model #2. In Model #2, Equation 2-6 is used again, but this time the roll of webbing is assumed to act like multiple independent cylinders added together rather than one solid cylinder. To find the buckling force of each layer, the material properties from Table 4-5 were used along with a thickness of the web, .00142 in. The comparison of the values found using Model #2 to the experimental data can be seen in Figure 5-4.

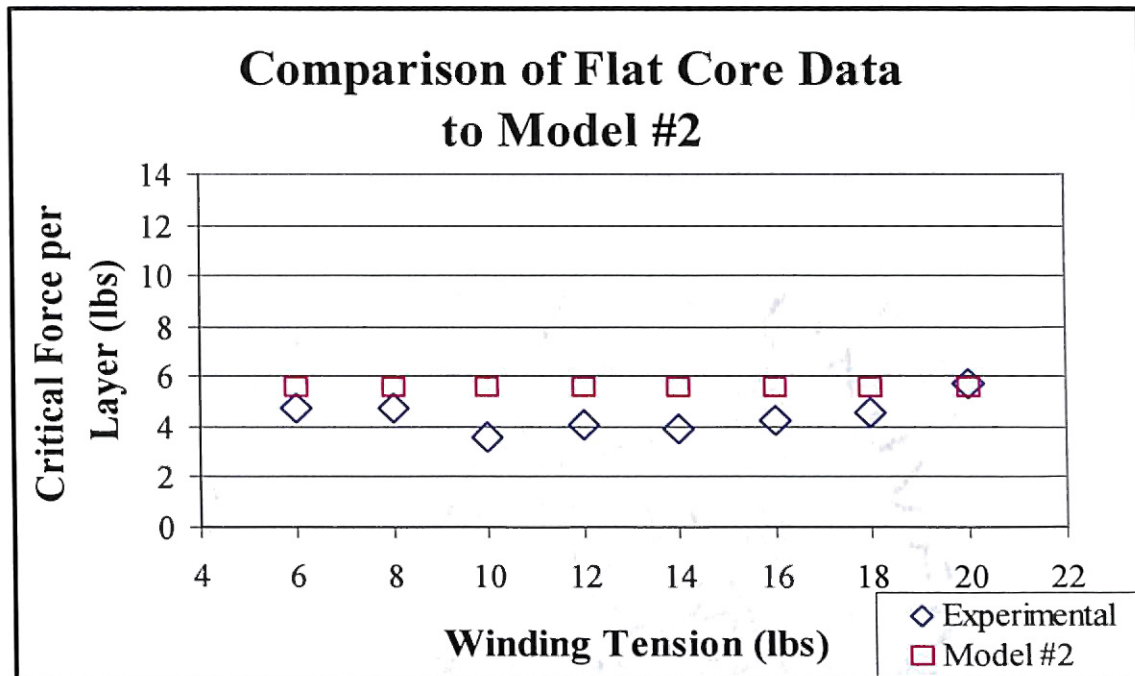


Figure 5-4: Comparison of Experimental Flat Core Data to Model #2

As can be seen above, the experimental *data matches* Timoshenko's equation much better when Model #2 is employed in which each web layer is assumed to buckle independently. Winding tension does not seem to affect the amount of force needed to buckle the roll, at least not in a simple fashion. The varying and reduced critical loads found experimentally are most likely due to imperfections in the roll. In Timoshenko [2], it is stated that *any imperfection* in the cylindrical shape will cause the critical buckling force to reduce. Furthermore, the slight increase in *buckling force at higher tensions is* most likely due to the *testing apparatus*. At the higher tensions, the web that laid over the *gap region tended to pull into the gap*. As tension increased, more 'pull in' would occur. It is likely that as a roll was *compressed, the web that was pulled into the gap region* would interfere with the movement of the core causing an increase in *critical force*. An example photo of the imperfections seen in the web rolls after winding can be seen in Figure 5-5.

All of the remaining models grossly over-predicted the buckling load, and therefore they will not be shown in comparison to experimental data found using the flat core. (However, these models can be seen in comparison to the toothed cores in the following section.)



**Figure 5-5: Imperfections Seen in Rolls after Winding**

### **Toothed Core Analysis and Discussion**

The toothed cores were designed to only allow for buckling in one direction: outwards. In addition, these cores did not allow the roll to twist along the axis when being crushed. Therefore, these rolls buckled in the shape of outward ridges. However, due to the differences in gap size, the two cores did have some variations in buckling shapes.

As mentioned in the ‘Experimental Setup and Procedure’ chapter, two sets of eight tests were conducted on toothed core #1. Following the tests conducted on the flat core, the only input that was varied from test to test was the tension (6 lbs to 20 lbs.) Due to the large gap sizes in toothed core #1, some problems were observed while testing it.

During several of the tests, while a roll was being crushed, areas of early buckling could be seen in the gaps. An example of this pre-buckling can be seen in Figure 5-6. Then, as the roll proceeded to be crushed, the expected buckle shape would occur at the gap region of the core. On other tests, the roll would not pre-buckle and instead it would only form the expected ridge buckles, but even on these tests, the buckles occurred at the gap regions. An example of the main buckle can be seen in Figure 5-7.

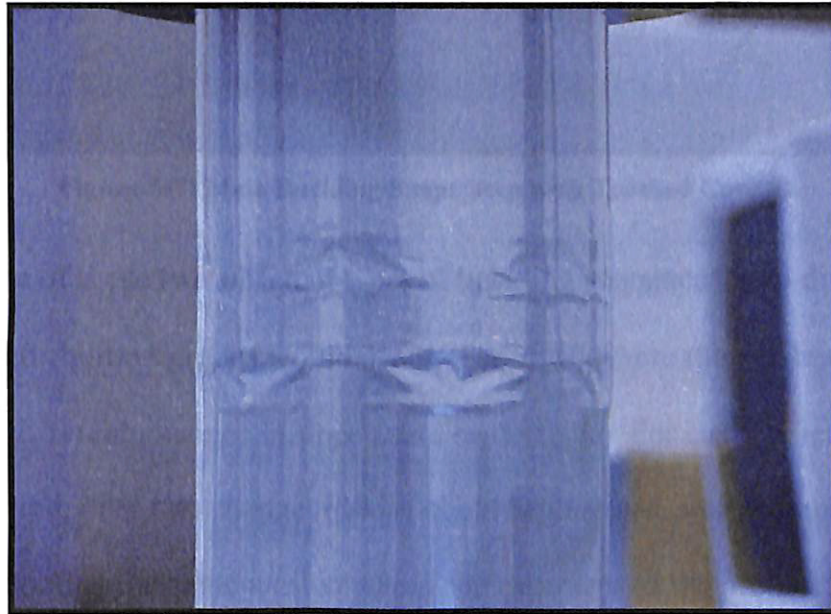


**Figure 5-6: Pre-buckling that Occurs in the Gaps of Toothed Core #1**

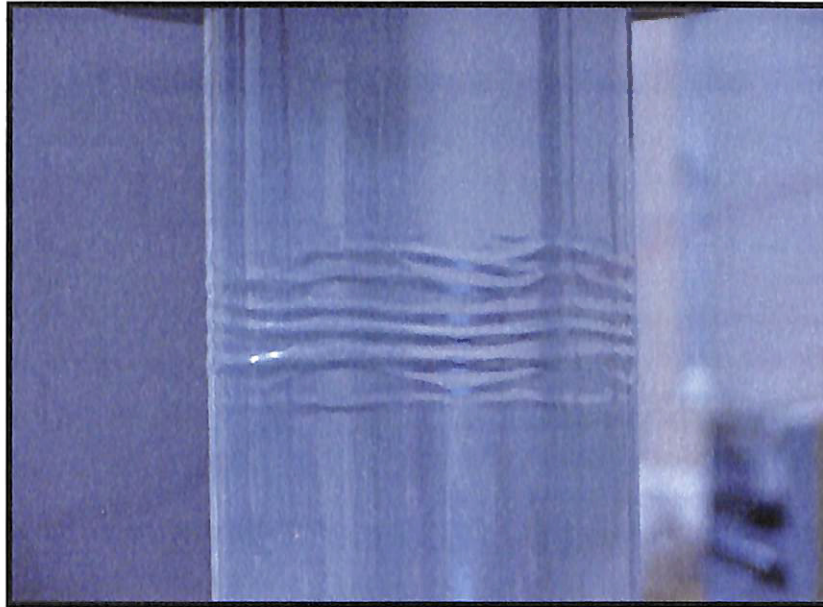


**Figure 5-7: Main Buckling Shape Seen with Toothed Core #1**

Because of these two different types of buckling sequences, two different types of force versus deformation graphs would occur. For cases where the pre-buckling occurred, two different changes in slope could be detected. For cases where no pre-buckling occurred, only one change in slope could be detected. An example comparison of two tests wound at the same tension where one experienced the pre-buckling and one did not can be seen in Figure 5-8.



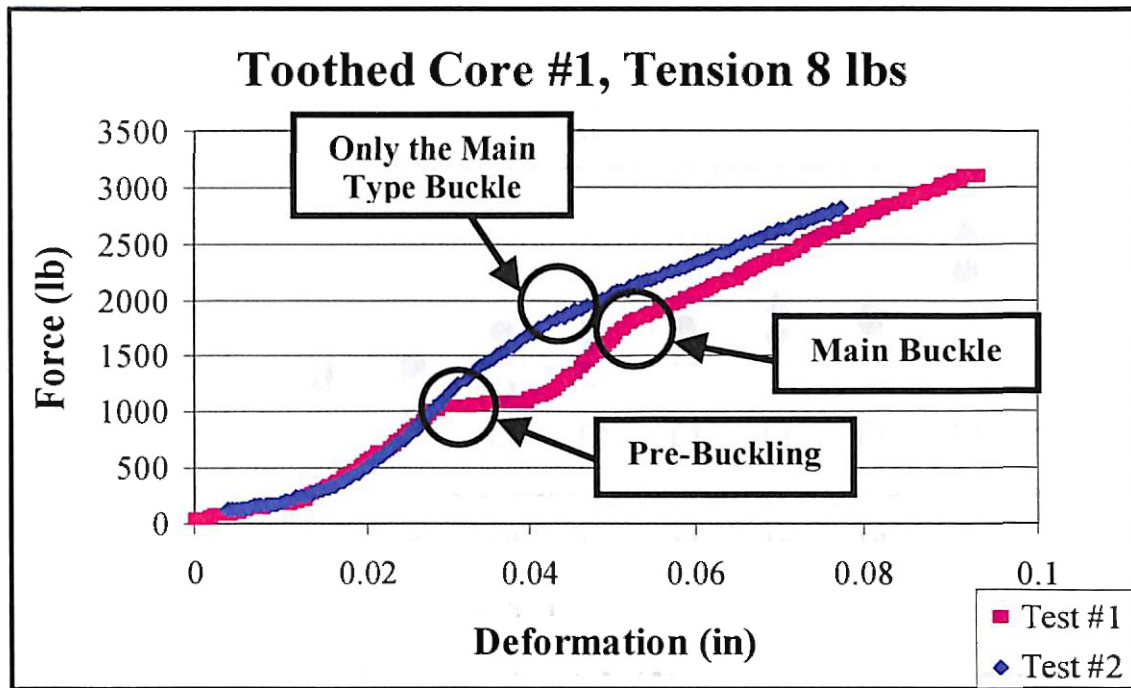
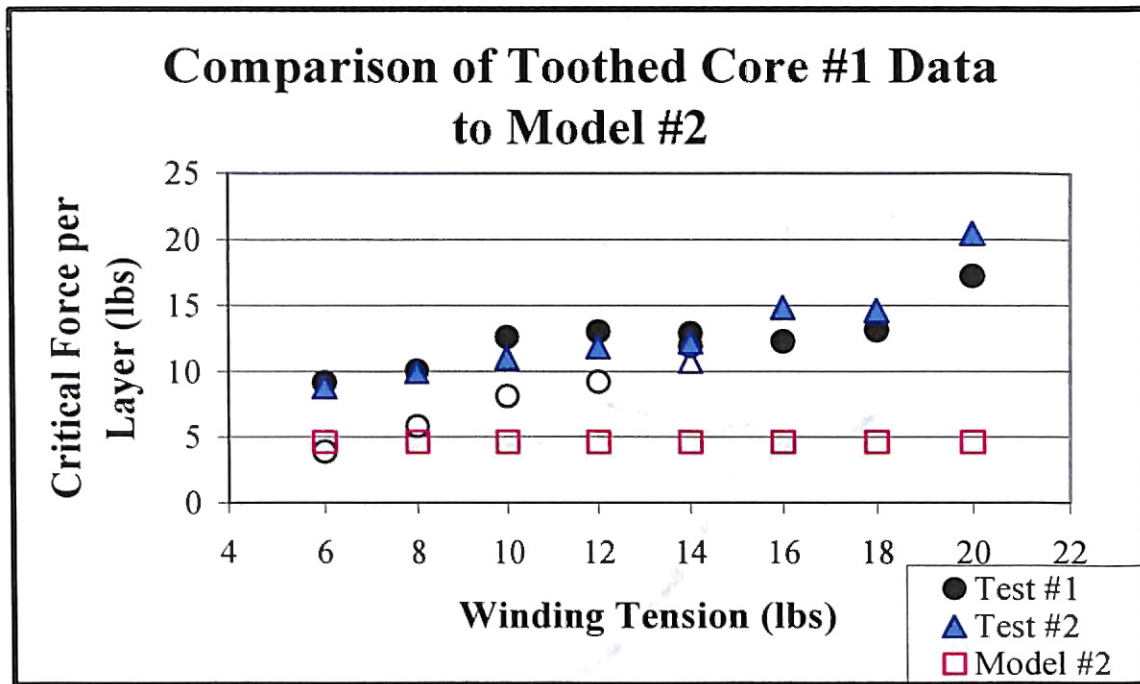


Figure 5-8: Example Buckling Curves for Toothed Core #1

It is interesting to note that for either case, the roll continues to hold higher loads even after it buckles. This shows that even though the roll has changed shapes to find a lower state of energy, the new shape still gives support to the applied force. The critical force is found by fitting lines to each section of the curve. The deformation at which these lines cross defines the deformation at which buckling begins. The critical force of buckling is then found by determining the force which corresponds to the deformation at which buckling began.

For each test run on toothed core #1, the pre-buckle and main buckle critical forces were recorded if both occurred. Otherwise, the one critical main buckling force was recorded. In Figure 5-9, the results of the two sets of tests run on the toothed core #1 can be seen. Lower points that are hollow but of the same shape and color of higher points indicate critical points where pre-buckling occurred.



**Figure 5-9: Comparison of Toothed Core #1 Data to Model #2**

Reviewing Figure 5-9, it is clear that Model #2, which uses Timoshenko's equation for the buckling of a cylinder, does not match the experimental data. The data presented would support the observation that as the winding tension is increased the force needed to buckle the cylinder also increases. However, since the cylinders sometimes pre-buckle, the results from these experiments may be faulty. Likewise, as mentioned earlier, the buckles only occur in the region where the gaps exist. This raises the question of whether the gap size of the core is affecting the results. Therefore, the second toothed core was designed with smaller gaps. Since the web cylinder usually buckled within .10 inches, the new gap was made to be slightly larger, .15 inches.

This new core, toothed core #2, was tested in the same manner as the previous two cores. One set of tests was run where tension was the only input varied (6 lbs to 20 lbs.). As expected, this core resulted in much better data. Pre-buckling no longer

occurred during any test with toothed core #2. An example force curve can be seen in Figure 5-10, and an example photograph of the buckled shape can be seen in Figure 5-11.

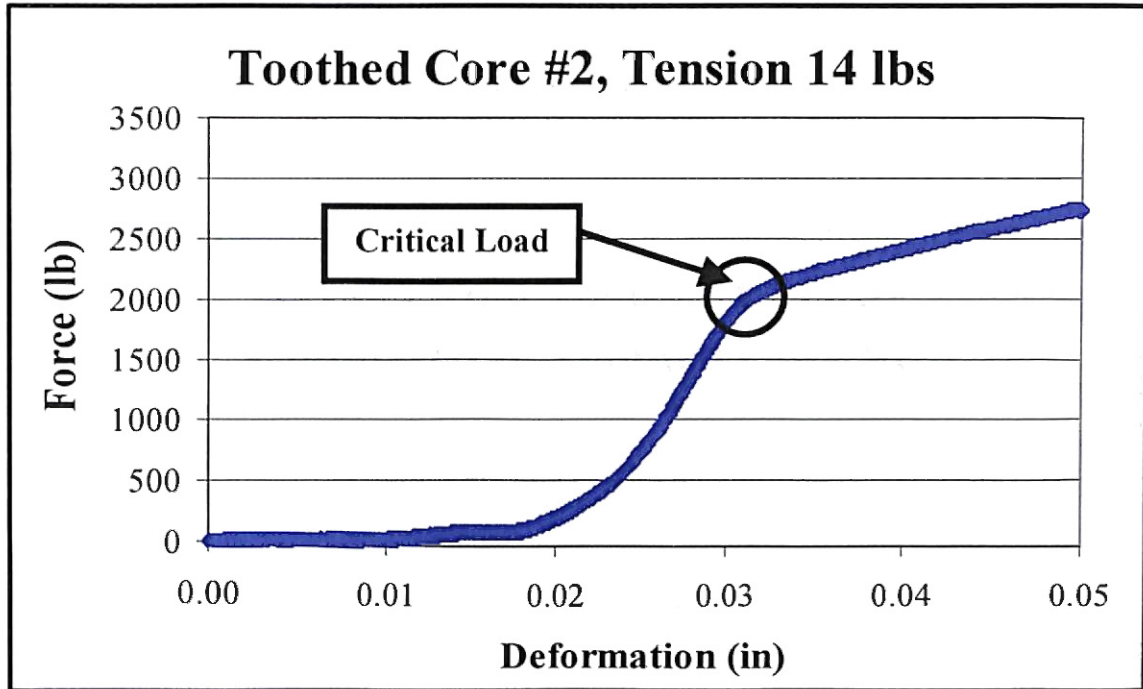


Figure 5-10: Example Buckling Curve for Toothed Core #2

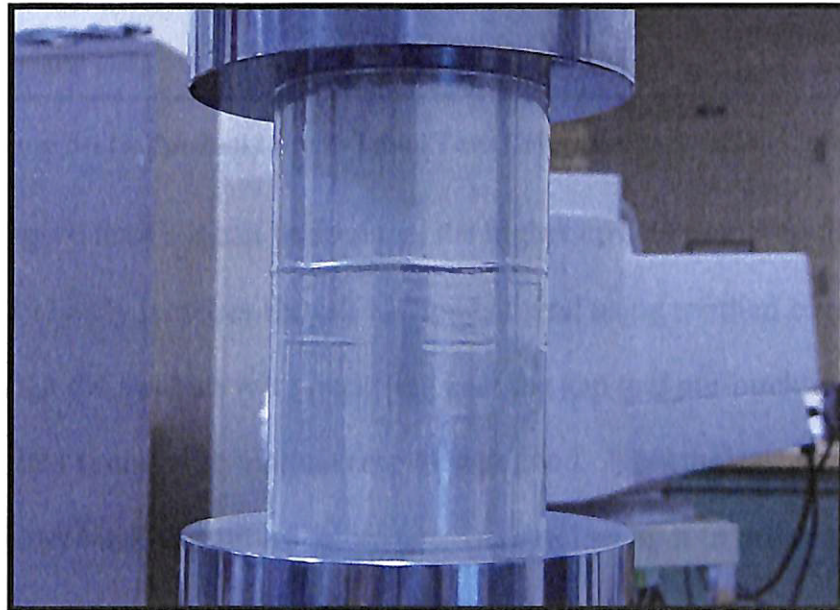


Figure 5-11: Buckle Shape Seen for Test Conducted on Toothed Core #2

Figure 5-10 shows that the critical force at which the cylinder buckles is once again determined by finding the point at which the slope changes. It should be noted that the cylinder continues to support higher forces even after being buckled as was seen with data from toothed core #1. Results from toothed core #2 were compared to the tests run on toothed core #1, seen in Figure 5-12.

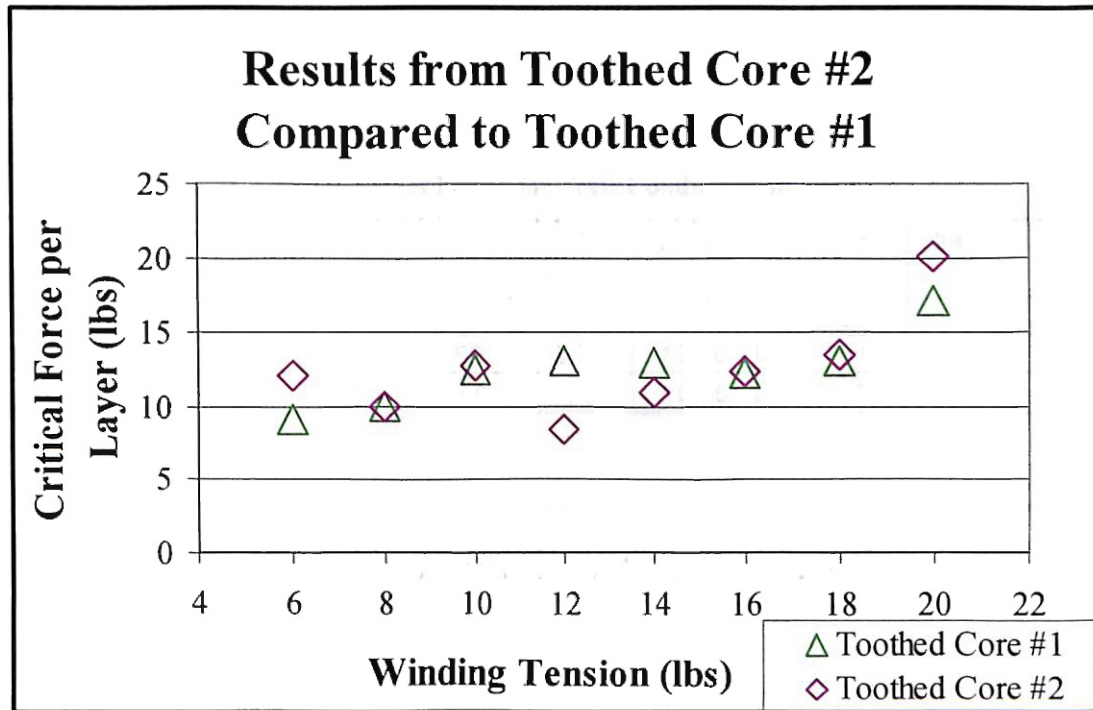


Figure 5-12: Toothed Core #2 Initial Tests Compared to Toothed Core #1

In the figure above it can be seen that the higher critical points found using toothed core #1 closely matches the critical points found using toothed core #2. Therefore, though the buckles were occurring near the gap and pre-buckling was occurring, the data found with toothed core #1 was good. Nonetheless, since toothed core #2 gave better buckling curves, more tests were run using it in order to collect data to use as a comparison to the theoretical models.

For these new sets of tests, a higher range of tensions was chosen. As can be seen in Figure 5-9 and Figure 5-12, the largest amounts of change in critical force occur at the

higher tensions. Therefore, the load cell of the winding machine was re-calibrated to measure tensions up to 26 lbs. Using toothed core #2, three sets of tests were completed in which tension was varied from 12 lbs to 26 lbs. The critical force determined for each test can be found in Table 5-3. The critical forces are given as force per layer for easier comparison. The average critical force is found for each value of tension. These average values will be used to compare experimental data to the developed theoretical models. A graph of these averages can be seen in Figure 5-13.

**Table 5-3: Critical Forces Found for Tests Conducted on Toothed Core #2**

Tension	12 lbs	14 lbs	16 lbs	18 lbs	20 lbs	22 lbs	24 lbs	26 lbs
Set 1 $N_{cr}/\text{layer}$	10.20	12.48	13.48	14.79	16.55	18.34	19.70	20.16
Set 2 $N_{cr}/\text{layer}$	9.92	11.72	13.25	14.77	17.02	18.63	19.80	20.61
Set 3 $N_{cr}/\text{layer}$	8.70	9.73	11.59	13.72	15.50	17.51	17.15	20.21
Avg. $N_{cr}/\text{layer}$	9.61	11.31	12.77	14.43	16.36	18.16	18.88	20.33

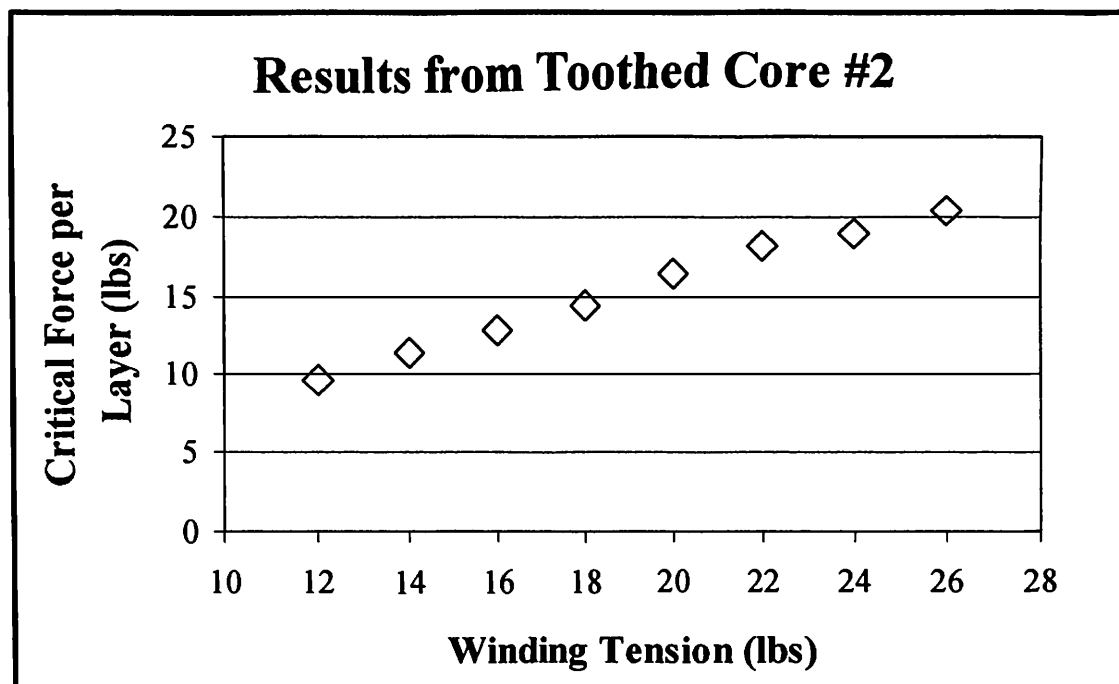


**Figure 5-13: Averaged Results of Toothed Core #2 Tests**

By reviewing this graph it appears that as winding tension increases, the force needed to buckle a roll of web increases. Furthermore, the relationship between winding

tension and critical force seems to be linear. Since neither Model #1 nor Model #2 considers winding tension, data from toothed core #2 will not be compared to them. Instead, Model #3 will first be used for comparison.

Model #3 uses the buckling equation for cylinders on an elastic foundation. In *this model the approach used* is similar to the one used by Forrest [4]. In this model, every layer is considered to act like a *cylinder on an elastic foundation*. *The foundation* for each cylinder is made up *of the layers below it*. Therefore, the buckling force for each cylinder is found using Equation 3-6 where the inputs for the *foundational stiffness* and radius are updated for each layer. To find the foundational stiffness for each layer, the radial elastic modulus is needed for each layer. This was found using the winding software as discussed in Chapter 4. The foundational stiffness is then found using Equation 3-8. Then, the buckling force for each layer is found using the calculated foundational stiffness and the material properties found in Table 4-5. A comparison of Model #3 to the experimental values of toothed core #2 can be seen in Figure 5-14.

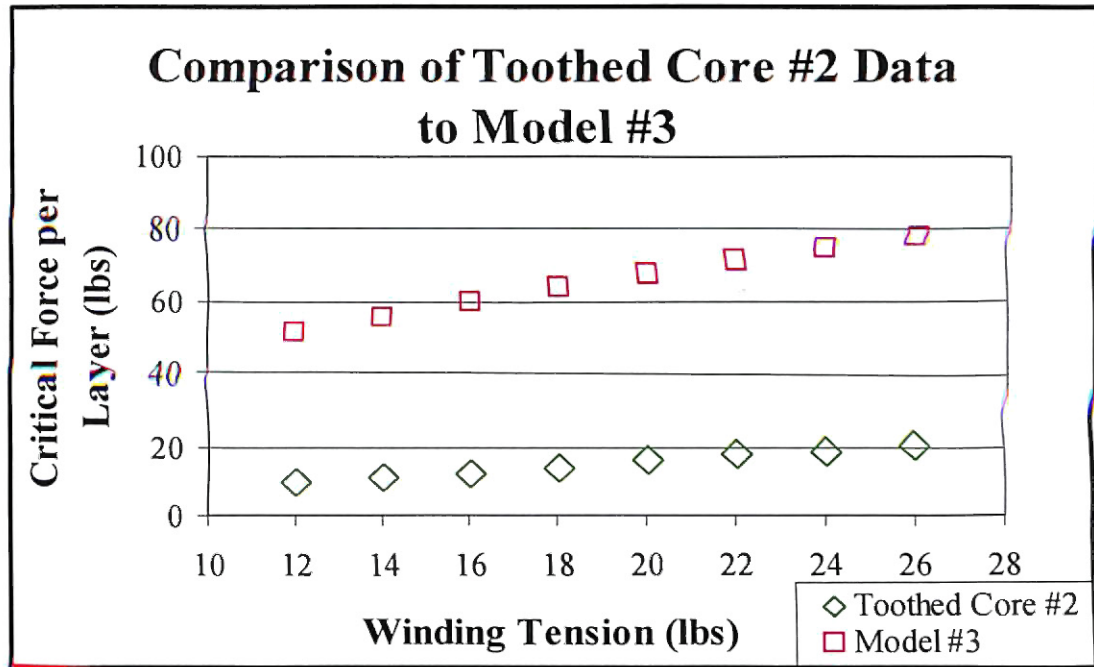


Figure 5-14: Comparison of Toothed Core #2 Data to Model #3

From this graph, it can be seen that Model #3 does not result in a solution that matches the experimental data. Model #3 results in values higher than the experimental values. Likewise, its values have a much different slope than the experimental values. Therefore, Model #3, the elastic foundation model, does not correctly describe the buckling of a roll of web.

As discussed in Chapter 3, all attempts using FEM programs to develop Model #4 were inconclusive. Therefore, Model #4 will not be used for comparison. Instead, Model #5 will now be compared to the results obtained from winding and buckling tests using toothed core #2. As mentioned earlier, the pressure at the core of the roll increases as a function of tension. Pressure values for the different winding tensions can be seen in Table 4-3. Using these pressures, the resulting hoop stress in the core can be found using Equation 2-13. Then, using Equation 3-9 the area of contact between the sides of the teeth was found to be  $.18 \text{ in}^2$ . Finally, using Equation 3-10, where the coefficient of

friction between two steel surfaces is .3, the frictional force between each tooth can be found. The total frictional force that would occur at each tension level for a roll with 177 layers can be seen in Figure 5-15.

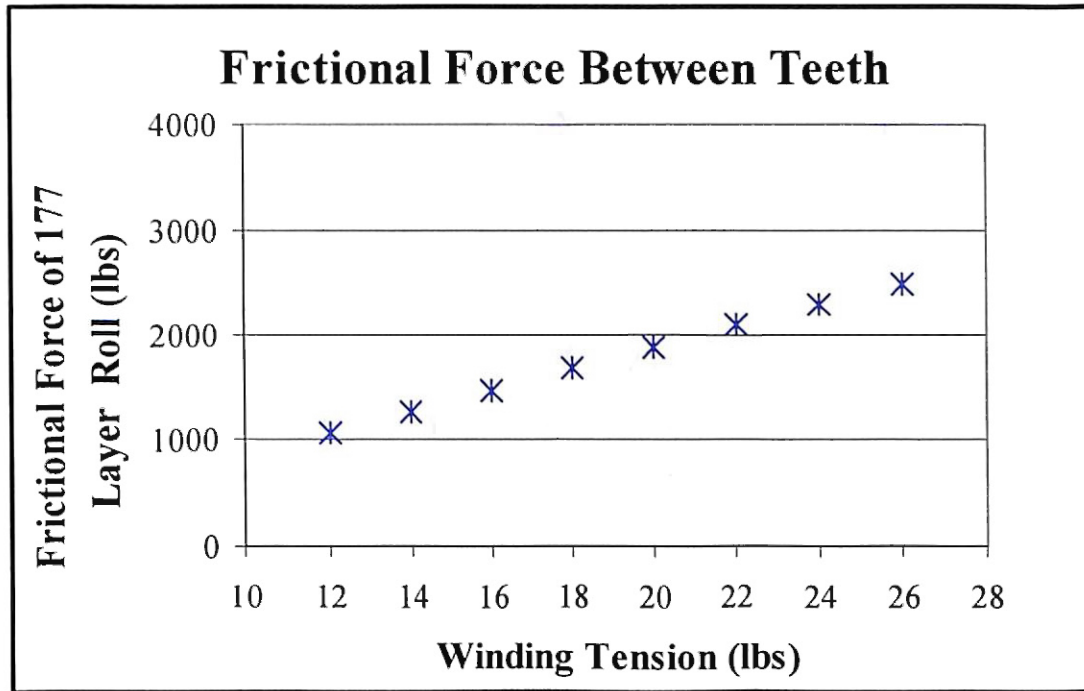


Figure 5-15: Frictional Force between the Teeth Compared to Web Tension

In Figure 5-15, it can be seen that the frictional force between the teeth is a large value and has a similar trend to the data found on toothed core #2. This frictional force was added to the critical force found using Timoshenko's buckling equation, Model #2, in order to calculate the critical forces for Model #5. A comparison of Model #5 to experimental data can be seen in Figure 5-16.



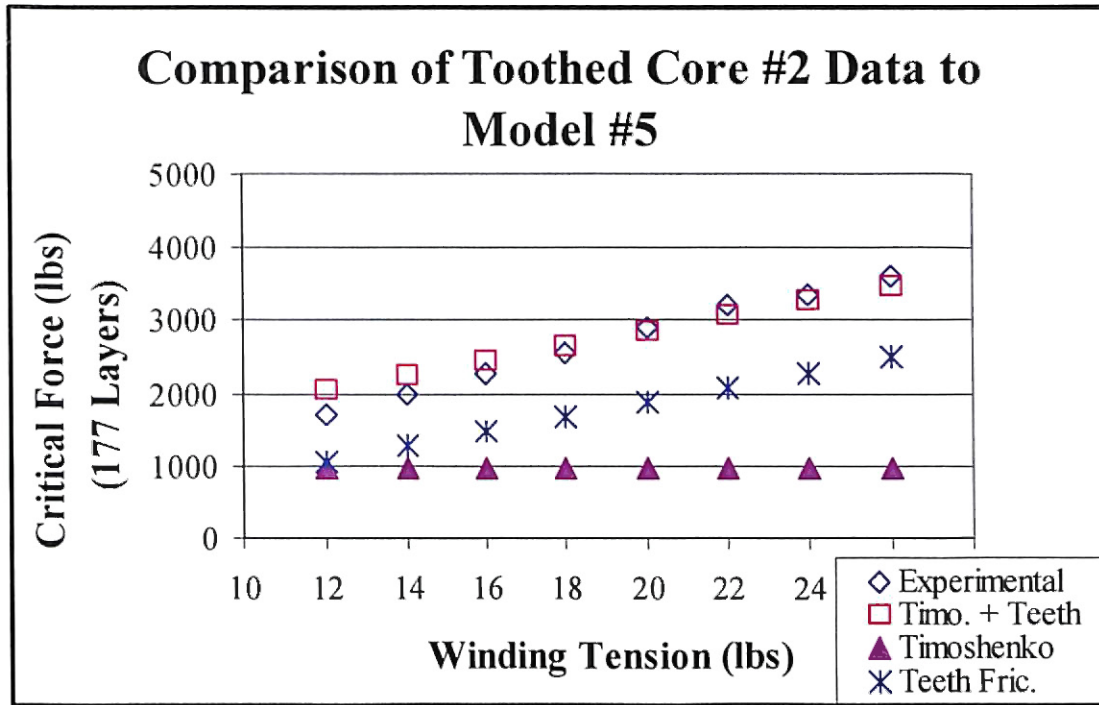


Figure 5-16: Comparison of Toothed Core #2 Data to Model #5

From this graph, it can be seen that Model #5 closely matches the experimental data quite well and, in fact, much better than any other model described here in. Thus, the assumption that the gaps between the sides of the teeth would close due to the pressure on the core was valid. It can be seen in the graph that some of the gaps between the sides of the teeth may not have closed at the lower pressures due to slight variations in the gap sizes. This would explain the slight difference in the experimental and theoretical data at the first few points. Nonetheless, from the comparison shown in Figure 5-16 it can be concluded that tension does not actually affect the buckling force. Instead, the tension affects the frictional force between the sides of the teeth through the resulting pressure on the core due to winding. Therefore, the critical force needed to buckle the web rolls wound on toothed core #2 can be solved using Timoshenko's theory once frictional effects have been considered.

However, in Model #5 the assumption was made that the one-way buckles that occur are simply one half of the two-way buckles assumed in Timoshenko's theory, and the length of the cylinder being buckled is equal to the length of the buckle. (With these assumptions, it was shown that Timoshenko's buckling equation could be used for one-way buckles.) If these assumptions are true, the length of the one-way buckles found experimentally should be equal to the theoretical length of the cylinder being buckled found using Equation 3-13. From Equation 3-13, using an average radius of 3.62 inches, the length for the cylinder being buckled was found to be .088 inches. For several of the tests conducted on toothed core #2 the length of the one-way buckle was measured. It should be noted that measuring the wavelength of the buckle was difficult since only one buckle was occurring. Therefore, distinguishing where the buckle began and ended proved to be difficult. Nonetheless, the average wavelength of the one-way buckles occurring in the experimentations was calculated to be .11 inches. Though this value is slightly larger than the expected length found using Equation 3-13, the value is close enough to validate the assumptions.

## CHAPTER 6

### CONCLUSIONS AND FUTURE WORK

#### **Conclusions**

Tests conducted on the flat core showed that the critical force was not affected by tension. In these tests, the core was free to rotate about the axis when buckling. The resulting buckling shape of tests conducted on this core was the chain-link pattern or 'chess board' buckle. By comparing the experimental data to Model #2, it was shown that the flat core data closely matched Timoshenko's equation for the buckling of cylindrical shells when each layer of web is assumed to act like independent cylinders.

Experimental tests conducted on the toothed cores seemed to show that winding tension played an important part in the buckling of the cylinder, but in actuality, the increase in buckling load in these tests was due to the testing apparatus. In these cases, the rolls always buckled in a 'ridge' shape. This buckling shape is commonly seen in industry in web rolls that have circumferential wrinkles.

The results of this research indicate that axially compressed wound rolls do not benefit from the additional stability of an elastic foundation. This contradicts the theory presented by Forrest. Results presented herein demonstrate that including the elastic foundation yields theoretical buckling loads 4 to 5 times that witnessed in tests. Instead, Timoshenko's equation for the buckling of cylindrical shells was shown to match the

experimental data once the frictional force between the teeth of the core was taken into consideration.

Furthermore, in this study, winding tension, and thereby radial elastic modulus, were varied over a substantial range (Table 4-3). At the close of this research, it appears in Figure 5-4 and in Figure 5-16, after friction effects are removed, that winding conditions do not affect the axial buckling load of wound rolls. It should be noted that this conclusion is limited to winding conditions where air entrainment is not a factor because the tests in the research were run at velocities and tensions that would prohibit air entrainment.

### **Future Work**

Finding an equation that predicts the amount of force needed to buckle a web roll is only the beginning step to preventing these wrinkles. Knowing the critical force at which these rolls buckle leads to the discovery of which internal factors within the roll could cause such forces. If the causes of these forces could be identified and prevented, circumferential wrinkles could then be avoided.

Before the search for the causes of these forces begins, it would also be a good idea to further test this model. In the future, other materials should be tested. Likewise, the same material with a different thickness should be tested. Such tests would help to prove the usability of this model.

## REFERENCES

- [1] Semiannual Technical Review and Industry Advisory Board Meeting Notes, "Mechanics of a Web during Winding". Oklahoma State University, October 2002 pp. 2.35-2.43
- [2] Timoshenko, S., Theory of Elastic Stability, 1<sup>st</sup> ed., McGraw Hill, New York, 1936
- [3] Allan, T., "One-Way Buckling of Elasticity Restrained Columns". Journal of Mechanical Engineering Studies, Vol. 11, No. 3, 1969
- [4] Forrest, A. W., "Wound Roll Stress Analysis Including Air Entrainment and the Formation of Roll Defects". Proceedings of The 3rd International Web Handling Conference, Oklahoma State University, Stillwater, OK, June 1995
- [5] Pfeiffer, J. D., "Internal Pressure in a Wound Roll of Paper". TAPPI Journal, Vol. 49, No. 8, August 1966, pp. 342-347
- [6] Allen, H.G. and Bulson, P.S., Background to Buckling, 1<sup>st</sup> ed., McGraw-Hill, New York, 1980
- [7] Shigley, J.E. and Mischke, C.R., Mechanical Engineering Design, 5<sup>th</sup> ed., McGraw-Hill, New York, 1989
- [8] Budynas, Richard G., Advanced Strength and Applied Stress Analysis, 2<sup>nd</sup> ed., McGraw-Hill, New York, 1999

VITA #1

John Michael Hix

Candidate for the Degree of

Master of Science

Thesis: A STUDY OF CIRCUMFERENTIAL WRINKLES THAT OCCUR IN ROLLS OF WEB

Major Field: Mechanical Engineering

Biographical:

Personal Data: Born in Tulsa, Oklahoma, on May 19, 1978, the son of Les and Joan Hix. Raised in Stillwater, Oklahoma. Married Tara Dean, on July 17, 1999

Education: Graduated from Stillwater High School, Stillwater, Oklahoma in May 1997; received Bachelor of Science degree in Mechanical Engineering from Oklahoma State University, Stillwater, Oklahoma in May 2002. Completed the requirements for the Master of Science degree with a major in Mechanical Engineering at Oklahoma State University in May 2004

Experience: Radio Shack, Stillwater, Oklahoma, May 1997 – December 2001; Undergraduate Research Assistant, Oklahoma State University, May 2001 – May 2002; Graduate Research Assistant, Oklahoma State University, May 2002 – December 2003; L-3 Communications, Greenville, Texas, January 2004

Honor Societies: Pi Tau Sigma Mechanical Engineering Honor Society, Tau Beta Pi Engineering Honor Society, Golden Key National Honor Society